International Journal of Multiphase Flow 146 (2022) 103853

Contents lists available at ScienceDirect

International Journal of Multiphase Flow

journal homepage: www.elsevier.com/locate/ijmulflow

Prediction of the liquid film reversal of annular flow in vertical and inclined pipes

Li-song Wang [a,b], Shuo Liu [b], Lin-tong Hou [a,b], Meng Yang [a,b], Jian Zhang [a,b], Jing-yu Xu [a,b,*]

[a] School of Engineering Sciences, University of Chinese Academy of Sciences, Beijing, 100049, China
[b] Institute of Mechanics, Chinese Academy of Sciences, Beijing, 100190, China

ARTICLE INFO

Keywords:
Churn flow
Intermittent flow
Liquid loading
Gas wells
Critical gas velocity

ABSTRACT

This work proposes a simplified model and a unified model to predict the critical gas velocities of film reversal based on the conservative momentum principle. The simplified model is expressed by an analytical solution of dimensionless form, while the unified model is presented by an iterative solution. The measured datasets of different pipe angles and diameters from the present and published works were used for model evaluation. The proposed simplified model is recommended to predict the film reversal because it can accurately predict the critical velocity with the total relative errors of 10.18% in the laboratory and 27.03% in the field, outperforming the unified model and published models. The unified model has a total relative error of 11.56% in the laboratory and 34.26% in the field. The contributions of the proposed two models are discussed by model comparisons. The results show that the simplified model integrates the merits of simple form and high accuracy; but, owing to the simplifications, the simplified model is not rigorous in the mechanism. In contrast, the unified model is more rigorous because it considers the interior liquid film viscosity, the droplet entrainment, and the non-uniform film thickness distribution in inclined pipes. The superiority of the unified model is discussed by comparing it with previous models in vertical and inclined pipes. The unified model contributes to understanding the underlying mechanism of film reversal. In general, the proposed simplified model and unified model complement each other to improve the prediction of the film reversal practically and theoretically.

1. Introduction

Annular flow is an important gas and liquid two-phase flow pattern that is widely encountered in industrial fields, such as the petroleum, chemical, and nuclear industries. At a high gas velocity, the annular flow is stable along with the characteristics of the liquid film around the pipe wall and the entrained droplets in the gas core. With the decrease in gas velocity, the annular flow begins to lose stability, and the liquid phase flows downward under the influence of gravity, leading to a transition from annular to intermittent flow (churn flow). This phenomenon could cause severe engineering problems in industrial applications, especially natural gas exploitation and production.

In the early stage of production, a high reservoir pressure means that the gas flow rate in the wellbore is also high, and the flow regime is a stable annular flow. However, the continuous depletion of the reservoir and decrease in formation pressure significantly decreases the gas velocity. The liquid phase begins to flow downward and accumulates at the well bottom, causing a decline in the production rate, even killing the well early (Lea and Nickens, 2004). This issue is called liquid loading in gas wells, which has drawn the attention of many researchers in recent years.

To mitigate the risk of liquid loading, several methods have been developed to predict its onset. Some studies have investigated liquid loading by transient modeling and laboratory tests from annular flow to churn flow because the liquid loading in gas wells is a transition of flow patterns (Alves et al., 2017; Tang et al., 2019; Waltrich et al., 2015a, 2015b). But the transient method has not been used widely in-situ because of its complex algorithm. One primary method in engineering applications is the analysis of steady annular flow to predict the critical gas velocity of liquid-phase reversal. The liquid-phase reversal in annular flow can be divided into two categories depending on the assumptions: the droplet reversal model and the liquid film reversal model. The droplet reversal model assumes that liquid loading occurs when the largest droplet in the annular flow starts to flow downward. The liquid film reversal model assumes that the reversal of the liquid film flow from upward to downward indicates the onset of liquid loading.

* Corresponding author at: Institute of Mechanics, Chinese Academy of Sciences, Beijing 100190, China.
E-mail addresses: liushuo@imech.ac.cn (S. Liu), xujingyu@imech.ac.cn (J.-y. Xu).

https://doi.org/10.1016/j.ijmultiphaseflow.2021.103853
Received 15 February 2021; Received in revised form 18 June 2021; Accepted 11 October 2021
Available online 13 October 2021
0301-9322/© 2021 Elsevier Ltd. All rights reserved.

Nomenclature

μ_l	liquid viscosity (Pa·s)
ρ_l	liquid density (kg/m^3)
r	radial distance from the center of the pipe (m)
V_l	liquid velocity (m/s)
$\frac{dP}{dz}$	pressure gradient (Pa/m)
g	acceleration of gravity (m/s^2)
β	pipe angle (degree, 90° is vertical).
V_{sl}	superficial liquid velocity (m/s)
D	pipe inner diameter (m)
ρ_g	gas density (kg/m^3)
δ_u	uniform film thickness (m)
τ_i	interfacial shear stress (Pa)
τ_w	wall shear stress (Pa)
f_i	interfacial friction factor
V_{sg}	superficial gas velocity (m/s)
$\frac{\delta_{min}}{\delta_{max}}$	the ratio between the minimum and maximum thickness
$V_{sg,c}$	measured critical gas velocity (m/s)
ε	absolute relative error (%)
N	number of data
K_p	predicted value
K_m	measured value

Dimensionless parameters

$\widetilde{V_{sl}}$	dimensionless superficial liquid velocity
$\widetilde{\delta_u}$	dimensionless film thickness
$\widetilde{\tau_i}$	dimensionless interfacial shear
$\widetilde{V_{sg}}$	dimensionless superficial gas velocity
$\widetilde{\delta_{max}}$	dimensionless maximum film thickness
$\widetilde{\delta_{eq}}$	equivalent film thickness

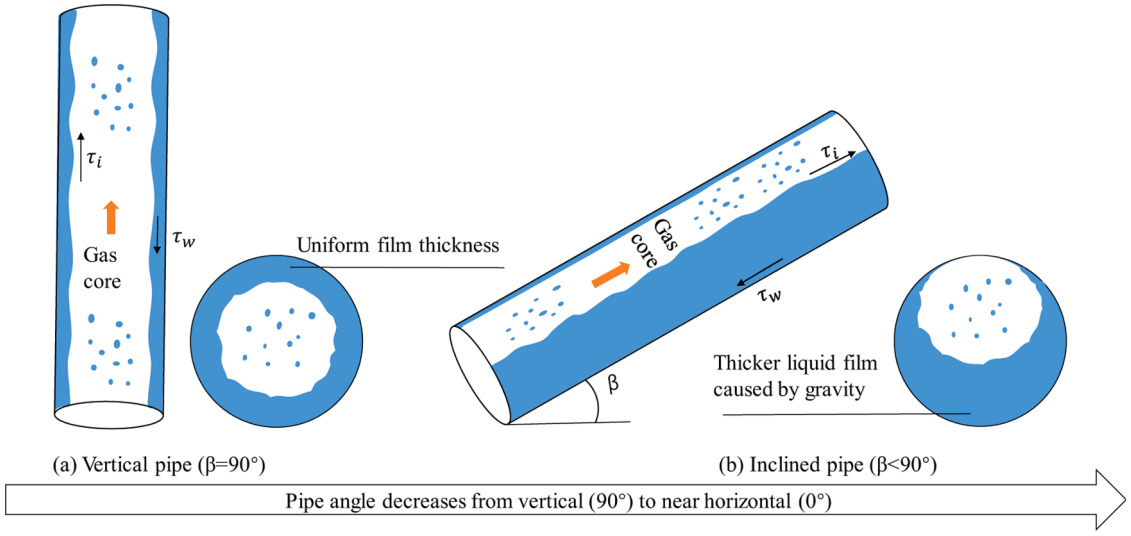

Fig. 1. Schematic of annular flow in vertical and inclined pipes.

Turner et al. (1969) proposed a droplet reversal model based on the mechanical equilibrium of a free-falling droplet, in which the critical gas velocity is considered to be equal to the free-fall terminal velocity of the maximum droplet in the gas core. They evaluated the model using field data and confirmed the validity of the droplet reversal model for identifying liquid loading. Because the droplet model of Turner et al. (1969) is simple and verified by field cases, it has been widely used for liquid loading prediction. Subsequent studies modified the droplet reversal model to improve its effectiveness (Belfroid et al., 2008; Coleman et al., 1991; Guo et al., 2006; Nossier et al., M.A. 2000). However, doubts have long been raised about the droplet reversal mechanism because of the lack of laboratory observations and verification. Van 't Westende et al. (2007) measured the size and velocity of droplets in annular flow under the liquid downflow condition, and found that the droplet size measured in the laboratory is much smaller than the maximum droplet size assumed in the Turner et al. (1969) model, which makes droplet reversal unlikely to occur in pipes. Experimental studies and transient modeling of liquid loading have also shown that, compared with the droplet reversal model, the models based on film reversal theory were more accurate to recognize the reversal of liquid phase (Alsaadi et al., 2015; Guner et al., 2015; Skopich et al., 2015; Veeken et al., 2009). These findings demonstrate the feasibility of predicting the critical gas velocity based on the film reversal mechanism instead of the droplet reversal theory.

A number of film reversal models have been proposed to predict the critical gas velocity and identify liquid loading in gas wells (Fan et al., 2018; Liu et al., 2018; Ratosgi and Fan, A. 2020; Wang et al., 2018). Among the existing models, a principal mechanism of film reversal is the stability analysis of the liquid film in annular flow. Taitel et al. (1982) analyzed the flow direction of a liquid film in vertical pipes, and showed that film reversal occurred as the liquid film began to lose stability, where the interfacial shear to keep liquid film flow upward was the minimum value. Barnea (1986) used a similar theory to study the transition between annular and intermittent flow. A film reversal model was proposed based on the force balance of the liquid film in annular flow. The Barnea (1986) model has been widely used to predict film reversal and liquid loading in gas wells, and many improvements have been made to this model in later studies (Luo, 2013; S. Luo et al., 2014; J. Li et al., 2014; Pagou et al., 2020; Shekhar et al., 2017).

However, compared with the droplet reversal model, the film reversal model is more complex because some input parameters are difficult to be measured by experiments or be calculated by empirical correlations. This impedes the general use of existing film reversal models, although it has been proved that the film reversal mechanism is

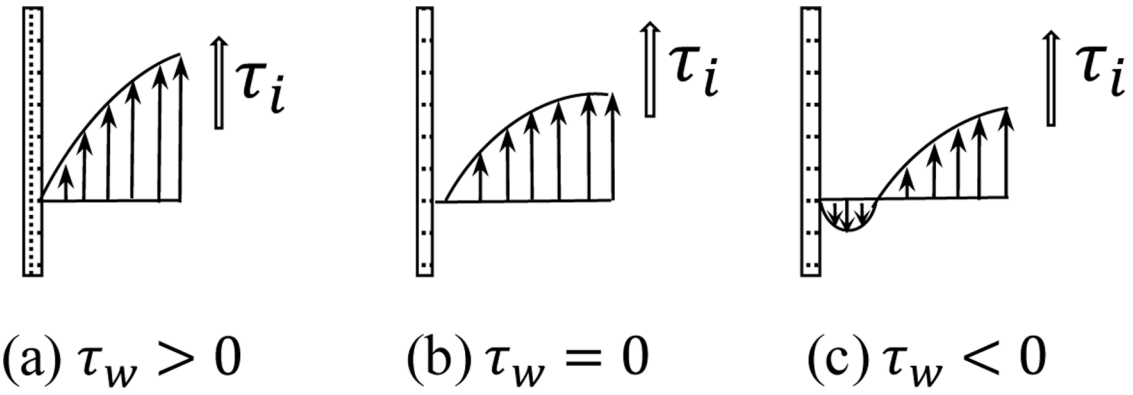

Fig. 2. Zero wall shear condition of film reversal.

capable of predicting gas velocity. Hence, it is necessary to propose a method that integrates accurate prediction and simple form.

The work aims to develop improved models to predict the film reversal accurately and conveniently in vertical and inclined pipes. By the conservation of momentum, this study proposes two approaches to predict film reversal: a simplified model and a unified model. The simplified model ignores some parameters to obtain an analytical solution of dimensionless form. The unified model is established rigorously without much simplification but with an iterative solution. Then, laboratory experiments are conducted for model evaluation. The proposed and published models are evaluated using experimental datasets from the present and previous studies. Finally, the features and contributions of the proposed two models are discussed by model comparisons.

2. Models establishment

2.1. Basic assumptions

Fig. 1 shows a schematic of the annular flow in the vertical and inclined pipes. Fig. 1(a) shows that the liquid film in vertical pipes distributed uniformly around the pipe wall. In the inclined pipes, the film at the bottom is thicker owing to the effect of gravity, while the film at the top is thinner, as depicted in Fig. 1(b). In vertical pipes, a model with a uniform film thickness can be obtained by modeling the film motion directly. In inclined pipes with non-uniform film thickness, the critical velocity can be calculated by introducing the angle correction relation. In the following subSection 2.2 and 2.3, a simplified model with the analytical solution and a unified model with the iterative solution are proposed, respectively. To establish the two models, steady, laminar, and incompressible liquid film was assumed, which has been proven in previous studies to be reliable for studying the film in annular flow (Barnea, 1986; Taitel et al., 1982).

2.2. A simplified model with the analytical solution

In the simplified approach, the zero wall shear criterion is used as the critical condition of film reversal. A schematic of the zero wall shear criterion is shown in Fig. 2, where τ_w is the wall shear stress and τ_i is the interfacial shear stress. When the film flows upward, the velocity distribution of the liquid film is upward, and the wall shear is positive, as shown in Fig. 2(a). When film reversal occurs, the velocity distribution near the pipe wall decreases, and the wall shear stress becomes negative, as shown in Fig. 2(c). Thus, a zero wall shear indicates the onset of film reversal (Turner et al., 1969), as shown in Fig. 2(b).

Under the axial symmetry condition, the momentum equation of the liquid film around the pipe wall is given as

$$\frac{\mu_l}{\rho_l}\frac{1}{r}\frac{\partial}{\partial r}\left(r\frac{\partial V_l}{\partial r}\right)-\frac{1}{\rho_l}\frac{dP}{dz}-g\sin\beta=0 \tag{1}$$

where μ_l is the liquid viscosity (Pa·s), ρ_l is the liquid density (kg/m^3), r is the radial distance from the center of the pipe (m), V_l is the liquid velocity (m/s), $\frac{dP}{dz}$ is the pressure gradient (Pa/m), g is the acceleration of gravity (m/s^2), and β is the pipe angle (degree, 90° is vertical).

Eq. (1) is the basic formulation to derive the simplified model. To describe the model concisely, the important equations of dimensionless form are presented here, and the detailed derivation procedures are presented in Appendix A.

Eq. (2) illustrates the relationship between the dimensionless superficial liquid velocity and the dimensionless uniform film thickness at the critical condition of zero wall shear.

$$\widetilde{V_{sl}}=2\sin\beta\left[1-4\left(\widetilde{\delta_u}-\widetilde{\delta_u}^2\right)\right]\left(\frac{1}{64}-\frac{1}{4}\left(\frac{1}{2}-\widetilde{\delta_u}\right)^4-\frac{1}{4}\left(\frac{1}{2}-\widetilde{\delta_u}\right)^2\ln\frac{1}{1-2\widetilde{\delta_u}}\right) \tag{2}$$

where $\widetilde{V_{sl}}$ is the dimensionless superficial liquid velocity, and $\widetilde{\delta_u}$ is the dimensionless film thickness. Eqs. (3) and (4) are the expressions of $\widetilde{V_{sl}}$ and $\widetilde{\delta_u}$.

$$\widetilde{V_{sl}}=\frac{\mu_L}{D^2\left(\rho_l-\rho_g\right)g}V_{sl} \tag{3}$$

$$\widetilde{\delta_u}=\frac{\delta_u}{D} \tag{4}$$

where V_{sl} is the superficial liquid velocity (m/s), D is the pipe inner diameter (m), ρ_g is the gas density (kg/m^3), and δ_u is the uniform film thickness (m).

The interfacial shear stress between the gas core and liquid film is given as Eq. (5).

$$\widetilde{\tau_i}=\sin\beta\left(\widetilde{\delta_u}-\widetilde{\delta_u}^2\right)\left(1-2\widetilde{\delta_u}\right) \tag{5}$$

where $\widetilde{\tau_i}$ is the dimensionless interfacial shear, as shown in Eq. (6). The τ_i in Eq. (6) is the interfacial shear stress in Pa.

$$\widetilde{\tau_i}=\frac{\tau_i}{D\left(\rho_l-\rho_g\right)g} \tag{6}$$

To obtain the analytical solution, Eqs. (2) and (5) should be simplified. Using the Taylor expansion of $\ln\frac{1}{1-2\widetilde{\delta_u}}$ at $\widetilde{\delta_u}$=0, the Maclaurin expression of $\ln\frac{1}{1-2\widetilde{\delta_u}}$ can be obtained. Then, Eq. (2) can be expressed by Eq. (7).

$$\widetilde{V_{sl}}=2\sin\beta\left[\frac{1}{3}\widetilde{\delta_u}^3+o\left(\widetilde{\delta_u}^3\right)\right] \tag{7}$$

Eq. (5) can be described as Eq. (8).

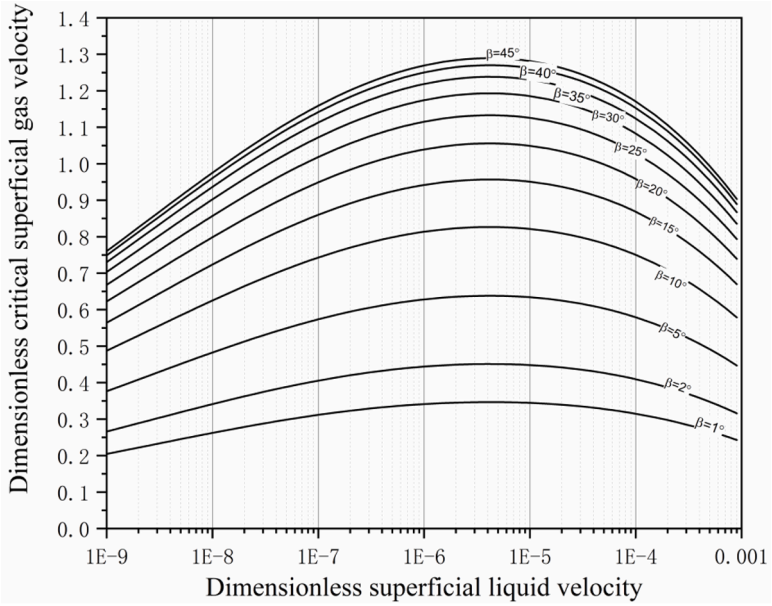

(a) Pipe angle ranges from 90° to 50°

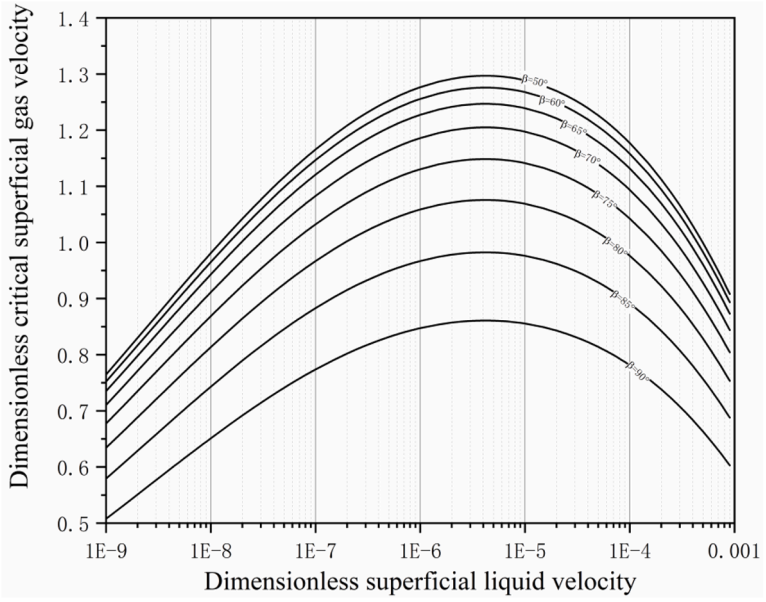

(b) Pipe angle ranges from 45° to 1°

Fig. 3. Dimensionless graphs of critical gas velocity by the simplified model.

$$\widetilde{\tau}_i = \sin\beta[\widetilde{\delta}_u + o(\widetilde{\delta}_u)] \tag{8}$$

Ignoring higher-order terms in Eqs. (7) and (8), the dimensionless liquid film thickness and interfacial shear in vertical pipes ($\beta = 90^{\circ}$) are simplified to Eqs. (9) and (10), respectively.

$$\widetilde{\delta}_u = \left(\frac{3}{2}\widetilde{V}_{sl}\right)^{1/3} \tag{9}$$

$$\widetilde{\tau}_i = \widetilde{\delta}_u \tag{10}$$

Substituting the Eqs. (9) and (10) into Eq. (11), the dimensionless critical gas velocity of film reversal with uniform film distribution can be obtained. Eq. (11) is derived from the relation between interfacial shear and gas velocity (Taitel et al., 1982).

$$\widetilde{V_{sg}} = \sqrt{\frac{2\widetilde{\tau}_i(1-2\widetilde{\delta}_u)^4}{f_i}} \tag{11}$$

where $\widetilde{V_{sg}}$ is the dimensionless gas velocity and f_i is the interfacial friction factor.

The dimensionless gas velocity is expressed by Eq. (12), where V_{sg} is the superficial gas velocity (m/s).

$$\widetilde{V_{sg}} = V_{sg}\sqrt{\frac{\rho_C}{D(\rho_L-\rho_C)g}} \tag{12}$$

The friction shear factor (f_i) in Eq. (11) is crucial for calculating gas velocity. Wallis (1969) proposed an interfacial friction factor that has been widely used for engineering applications. The studies by L.B. Fore et al. (2000) and Belt et al. (2009) illustrated that Wallis (1996) correlation can accurately predict the friction factor in the range of

$0.005 \le \widetilde{\delta_u} \le 0.02$, which covers most cases in the film reversal. Especially, as shown in Eq. (13), Wallis's (1969) correlation is an explicit formulation with respect to the dimensionless film thickness, so users can calculate the interfacial factor directly; hence, this correlation is used in the simplified model to obtain an analytical solution.

$$f_i = 0.005(1 + 300\widetilde{\delta_u}) \tag{13}$$

Combining Eqs. (9), (10), (11), and (13), the dimensionless critical gas velocity in vertical pipes can be given by Eq. (14).

$$\widetilde{V_{sg}} = \sqrt{\frac{2\left(\frac{3}{2}\widetilde{V_{sl}}\right)^{1/3}\left[1 - 2\left(\frac{3}{2}\widetilde{V_{sl}}\right)^{1/3}\right]^4}{0.005\left[1 + 300\left(\frac{3}{2}\widetilde{V_{sl}}\right)^{1/3}\right]}} \tag{14}$$

To consider the influence of non-uniform film thickness distribution in inclined pipes, a correction term must be introduced. Belfroid et al. (2008) proposed a simple angle correlation by the laboratory experiment. This correlation was validated by the field data with uncertainties of less than 20%, and its applicability ranged from horizontal to vertical pipes. Liu et al.'s (2018) investigation showed that Belfroid et al.'s (2008) correlation can be adopted in the film reversal model in the inclined pipe. However, the predictions with Belfroid et al.'s (2008) correlation result in overestimation in vertical and inclined pipes, as will be presented in Section 4.2. Hence, the Belfroid et al. (2008) correlation was modified to prevent the overestimation. Finally, we have the simplified model of the film reversal, as shown in Eq. (15).

$$\widetilde{V_{sg}} = \frac{\sin(1.78\beta)^{0.38}}{0.76}\sqrt{\frac{2\left(\frac{3}{2}\widetilde{V_{sl}}\right)^{1/3}\left(1 - 2\left(\frac{3}{2}\widetilde{V_{sl}}\right)^{1/3}\right)^4}{0.005\left(1 + 300\left(\frac{3}{2}\widetilde{V_{sl}}\right)^{1/3}\right)}} \tag{15}$$

Compared with previous film reversal models, the simplified film model is given by an analytical solution of dimensionless form. By introducing the dimensionless superficial liquid velocity and pipe angle, the critical gas velocity can be directly calculated using Eq. (15) to predict the onset of liquid film reversal. Additionally, because Eq. (15) is written in dimensionless form, dimensionless graphs can be obtained, as shown in Fig. 3. Notably, if the liquid film is large enough to block the gas core, then the annular flow may transform into intermittent flow before the critical gas velocity is reached. In this case, readers are suggested to refer to the flow regime transition mechanism in Barnea (1986).

2.3. A unified model with the iterative solution

The unified model can also be derived from Eq. (1). Concisely, the major formulations in the model are presented here, and the details of derivation are presented in Appendix B. Eq. (16) is the expression of dimensionless interfacial shear.

$$\widetilde{\tau_i} = \frac{(1 - 2\widetilde{\delta_u})}{2(\widetilde{\delta_u} - \widetilde{\delta_u}^2)^2}\widetilde{V_{sl}} + \sin\beta(1 - 2\widetilde{\delta_u})\left\{\frac{1}{4} + \frac{(1 - 2\widetilde{\delta_u})^2\left[(1 - 2\widetilde{\delta_u})^2 \ln\frac{1}{1 - 2\widetilde{\delta_u}} - 2(\widetilde{\delta_u} - \widetilde{\delta_u}^2)\right]}{16(\widetilde{\delta_u} - \widetilde{\delta_u}^2)^2}\right\} \tag{16}$$

To develop the unified model, we adopted the stability analysis in Barnea (1986) as the critical criterion. By equating the derivative of Eq. (16) with respect to $\widetilde{\delta_u}$ to zero, we have the relationship between the dimensionless superficial liquid velocity and dimensionless critical film thickness, as shown in Eq. (17). Given the dimensionless superficial liquid film velocity, the uniform film thickness of film reversal can be solved using Eq. (17) by trial and iterative methods.

$$\widetilde{V_{Sl}} = \sin\beta\frac{2(\widetilde{\delta_u} - \widetilde{\delta_u}^2)(2\widetilde{\delta_u}^4 - 4\widetilde{\delta_u}^3 + 7\widetilde{\delta_u}^2 - 5\widetilde{\delta_u} + 1) + \ln\frac{1}{1 - 2\widetilde{\delta_u}}(\widetilde{\delta_u}^2 - \widetilde{\delta_u} - 1)(2\widetilde{\delta_u} - 1)^4}{8(3\widetilde{\delta_u}^2 - 3\widetilde{\delta_u} + 1)} \tag{17}$$

In inclined pipes, the film around the pipe wall has a non-uniform distribution, as depicted in Fig. 1(b). Hence, the uniform thickness (δ_u) should be transformed to the maximum thickness (δ_{max}), in which the liquid film is prone to reverse initially. The maximum film thickness can be expressed as Eq. (18). The details of the angle correction procedure are shown in Appendix B.

$$\widetilde{\delta_{max}} = \frac{2\widetilde{\delta_u}}{1 + \frac{\delta_{min}}{\delta_{max}}} \tag{18}$$

where $\widetilde{\delta_{max}}$ is the dimensionless maximum film thickness; and $\frac{\delta_{min}}{\delta_{max}}$ is the ratio between the minimum and maximum thickness, which depends on laboratory tests and empirical relations. Previous relations of $\frac{\delta_{min}}{\delta_{max}}$ could lead to inaccurate predictions of the critical gas velocity (J. Li et al., 2014), especially at angles between 50° and 90° In this paper, a new empirical relation of $\frac{\delta_{min}}{\delta_{max}}$ is proposed based on a recently published experimental work on film thickness in inclined pipes (Freshtman et al., A. 2020). As presented in Eq. (19), this empirical relation has a simple form that depends only on the pipe angle. This angle correlation is discussed in Section 5.2.1.

$$\frac{\delta_{min}}{\delta_{max}} = \exp\left[-3.44 \times 10^{-2}(90 - \beta)\right] \tag{19}$$

Then, the maximum interfacial shear ($\widetilde{\tau_{max}}$) at the maximum film thickness ($\widetilde{\delta_{max}}$) can be calculated using Eq. (20), which is derived by combining Eqs. (16) and (17).

$$\widetilde{\tau_{max}} = \sin\beta\left(1 - 2\widetilde{\delta_{max}}\right)^3\left[\frac{\ln\frac{1}{1 - 2\widetilde{\delta_{max}}}\left(1 - 2\widetilde{\delta_{max}}\right)^2 + 2\left(\widetilde{\delta_{max}}^2 - \widetilde{\delta_{max}}\right)}{4\left(\widetilde{\delta_{max}}^2 - \widetilde{\delta_{max}}\right)\left(3\widetilde{\delta_{max}}^2 - 3\widetilde{\delta_{max}} + 1\right)}\right] \tag{20}$$

Introducing $\widetilde{\tau_{max}}$ back to Eq. (16), the equivalent film thickness $\widetilde{\delta_{eq}}$ can be obtained. Finally, substituting the maximum interfacial shear at the bottom ($\widetilde{\tau_{max}}$) and the equivalent film thickness ($\widetilde{\delta_{eq}}$) into the formulation of gas velocity (Eq. (11)), the critical gas velocity of the film reversal by the unified model can be calculated.

Wallis's (1969) friction factor shown in Eq. (13) is adopted in the unified model. It should be noted that the dimensionless film thickness used in the friction factor should be the dimensionless equivalent film thickness ($\widetilde{\delta_{eq}}$). A discussion of the accuracy of friction factors will be presented in Section 5.2.2, and results show that Wallis's (1969) correlation results in an error of 11.56%, outperforming other interfacial factors.

Compared with the fully developed annular flow, measuring the entrainment fraction for film reversal is difficult. An available entrainment correlation of film reversal was proposed by Barbosa et al. (2002). The overall error of this correlation is approximately equal to ±18.9%. However, it should be noted that Barbosa et al.'s (2002) correlation is fitted in vertical pipes and valid for 0.0127 m < pipe ID < 0.0508 m, which could not meet the requirements of various pipe diameters and angles. Magrini et al. (2012) evaluated Wallis's (1968) correlation by abundant laboratory datasets, including the fluids of air/water/oil, pipe diameters ranging 0.0231 m to 0.1 m, superficial gas velocities from 2.7 m/s to 166 m/s, superficial liquid velocities ranging from 0.007 m/s to 5.11 m/s, and pipe angles from 0° to 90° It was concluded that Wallis's (1968) correlation was recommended to calculate entrainment fraction because it had average absolute relative errors of 33.7% in vertical pipes and 30.0% in inclined pipes. Hence, Wallis's (1968) correlation of

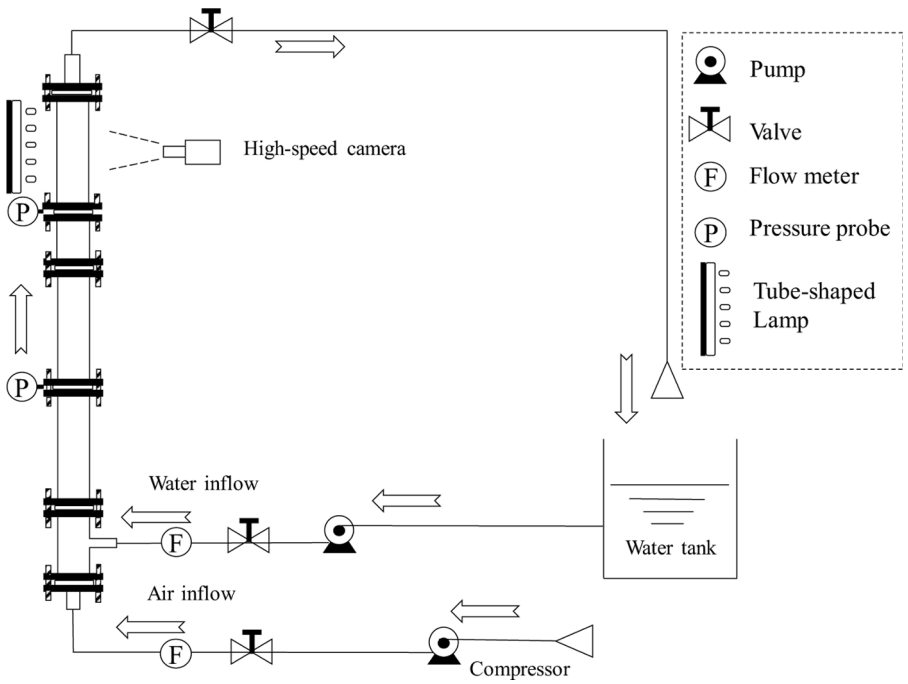

Fig. 4. Schematic of the laboratory experiment.

entrainment fraction is used in the unified model, as presented in Appendix B. Although Wallis's (1968) correlation is proposed for fully developed annular flow, it shows a great capacity of predicting film reversal, as will be presented in Section 5.1.2.

3. Model evaluation

3.1. Laboratory experiment

3.1.1. Experiment facility

Laboratory experiments were conducted to evaluate the proposed model. The current experiment aims to observe the film reversal process and determine the critical superficial gas velocity. Fig. 4 shows a schematic of the flow loop in the present study. The main test section is a plexiglass vertical pipe with a height of 3.2 m and inner diameter of 50 mm. The liquid and gas phases were tap water and compressed air, respectively. A compressor injected air into the test section at the bottom of the pipe, while a plunger pump introduced water into the pipe from a large water tank. A turbine flowmeter with a measuring range of 0–1 m^3/h and a float flowmeter with a range of 0–180 m^3/h were used to measure the flow rates of water and air, respectively. The entrance of the water was located in a 20 cm T-type junction up to the air entrance. Water and air were mixed in the T-type junction, which then flowed upward as a mixture. At the end of the test pipe, air was released into the atmosphere, and water was collected in the tank for cycling. Twenty-four tests were conducted at the facility. The experimental superficial liquid velocities were 0.1, 0.2, 0.3, 0.5 m^3/h (0.014, 0.028, 0.042, 0.071 m/s). The superficial gas velocities were 60, 80, 100, 120, 140, 160 m^3/h (22.64, 19.81, 16.98, 14.15, 11.32, 8.49 m/s). A high-speed camera was used to observe the flow regime and record the film reversal process. A tube-shaped lamp was placed behind the pipe to provide sufficient light for observation. Two probes were used to measure the flow pressure and obtain the pressure gradient. The distance between the two pressure probes was 1.5 m.

3.1.2. Flow reversal with decreasing gas velocity

Fig. 5 shows the film reversal process with decreasing gas velocity at the superficial liquid velocity of 0.014 m/s; the yellow arrows represent the flow direction of the liquid film. Fig. 5(a) shows that, when the gas velocity is 22.64 m/s, the liquid film flows upward at high speed. The liquid film thickness was smooth and thin, and the annular flow was stable. When the gas velocity decreased to 19.81 m/s, despite the presence of interfacial waves, the liquid film continued to flow upward, as shown in Fig. 5(b). When the gas velocity further decreased to 16.98 m/s, the liquid film flow fluctuated. Large waves frequently occurred, as shown in Fig. 5(c). The liquid film around this gas velocity was unstable because the interfacial wave stagnated and moved downward occasionally. Therefore, the onset of film reversal occurred at a gas velocity of around 16.98 m/s. The continuous decrease in the gas velocity to 14.15 m/s exacerbated the film reversal and interfacial waves, as shown in Fig. 5(d). At this time, it can be seen that the liquid film often flowed downward. However, the falling film flowed upward again when it encountered the large upward wave, similar to the observation in Guner et al. (2015). Therefore, despite the film reversal, the total liquid phase continued to flow upward. When the gas velocity decreased to 11.32 m/s, large waves occurred over the entire range of the liquid film, as presented in Fig. 5(e). The flow direction of the liquid film fluctuated up and down. The film thickness increased, making it difficult to retain the shape of the liquid film. At the lowest gas velocity of 8.49 m/s, the liquid film disappeared and the liquid phase oscillated at the pipe core as liquid blocks, as shown in Fig. 5(f).

Fig. 6 presents the flow observations at different superficial gas and liquid velocities. It can be seen that, with increasing superficial liquid velocity, the liquid film became thicker and the motion of interfacial waves intensified. Similar to the description in Fig. 5, at superficial gas velocities of 22.64 and 19.81 m/s, the annular flow at each superficial liquid velocity was stable and liquid film flowed upward. At superficial gas velocities less than 16.98 m/s, the backflow of liquid film was observed. At each superficial liquid velocity, interfacial waves in the liquid film stagnated and began to flow downward at the gas velocity range 14.15–16.98 m/s. The onset of film reversal occurred at this gas velocity range and the critical gas velocities were recorded, shown as the dashed line in Fig. 7.

The measured pressure gradients at each superficial liquid velocity are shown in Fig. 7. With the decrease in gas velocity, the pressure gradient first decreased and then increased after reaching a minimum

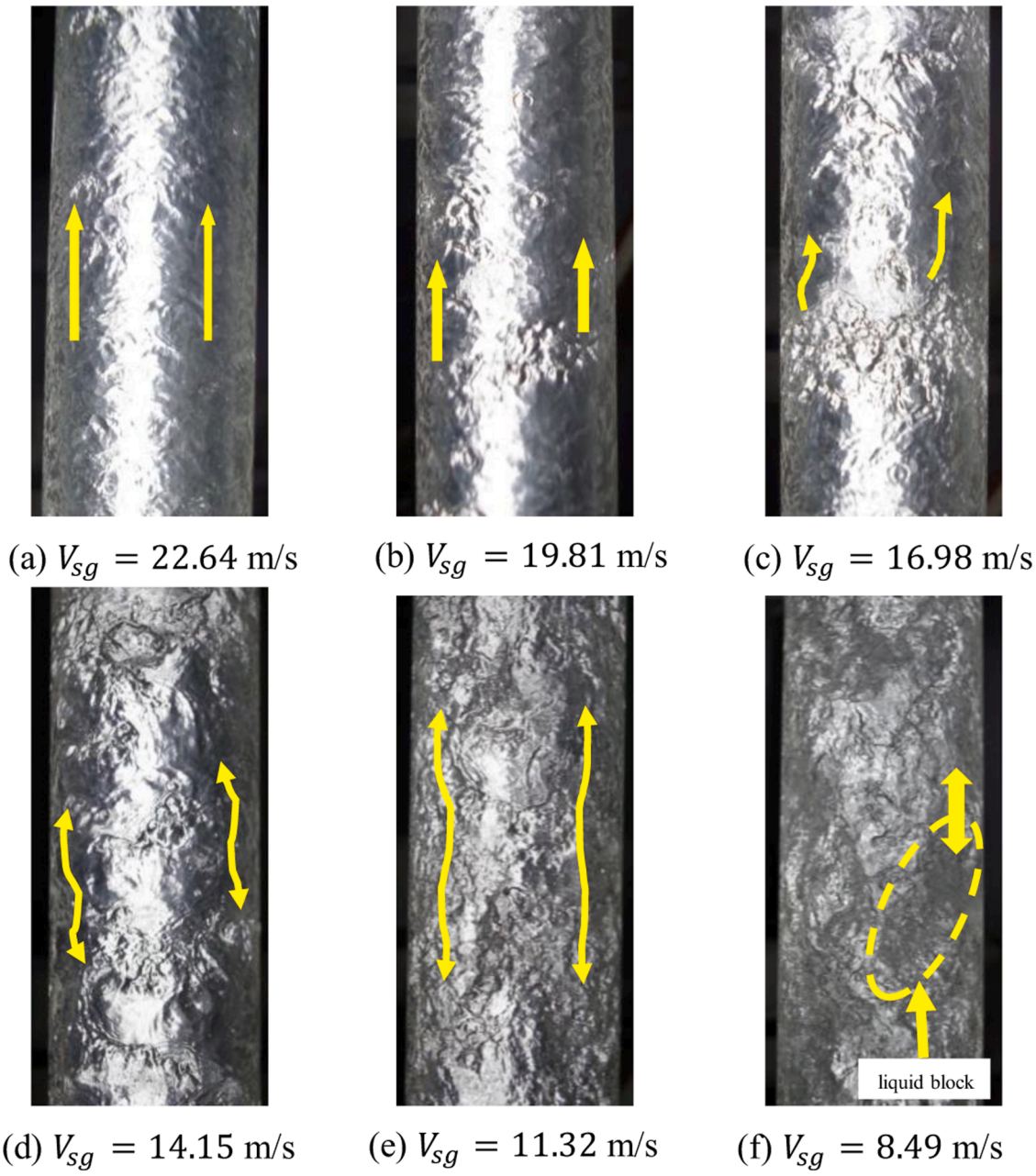

Fig. 5. Decreasing superficial gas velocity at V_{sl} = 0.014 m/s.

value. The occurrence of a minimum pressure gradient with the decrease of gas velocity owes to two opposing effects: gravitational gradient increasing and frictional gradient decreasing (assuming that the acceleration pressure gradient is ignored in cases of low liquid velocity). At the right of the minimum value, the total gradient was controlled by the friction gradient; hence, the total gradient decreased as the gas velocity decreased. At the left of the minimum value, the total gradient increased because the increasing gravity pressure gradient dominated the total pressure gradient. Fig. 7 shows that the minimum pressure gradient point occurred in the range 14.15–16.98 m/s when film reversal was observed to flow in reverse. At liquid velocities of 0.014 and 0.028 m/s, the observed critical gas velocity is slightly to the left of the minimum pressure gradient point. At liquid velocities of 0.042 and 0.071 m/s, the critical gas velocity occurred at the right of the minimum point. Previous studies have suggested that the identification of film reversal should depend on the motion of the film rather than the minimum pressure gradient point (S. Luo et al., 2014; Liu et al., 2018). Therefore, in this study, the observed film reversal is treated as the critical point, as plotted by the black points in Fig. 7.

3.2. Model evaluation with different datasets

3.2.1. Evaluation with experimental data in current and previous studies

Table 1 lists 85 experimental data collected from the present and previous studies. The pipe angles ranged from 1 to 90° (90° is vertical), covering the majority of inclined pipe angles. The pipe inner diameters ranged from 0.03 to 0.1524 m. The superficial liquid velocities were 0.001–0.1 m/s. To evaluate the adaptability of the proposed models, they were compared with seven published models. The model by Barnea (1986) is the most widely used basic model of film reversal, which is based on the stability analysis of annular flow. The S. Luo et al. (2014) model improved the Barnea (1986) model by considering the non-uniform film thickness distribution. J. Li et al. (2014) and Shekhar et al. (2017) advanced S. Luo et al. (2014) model by introducing

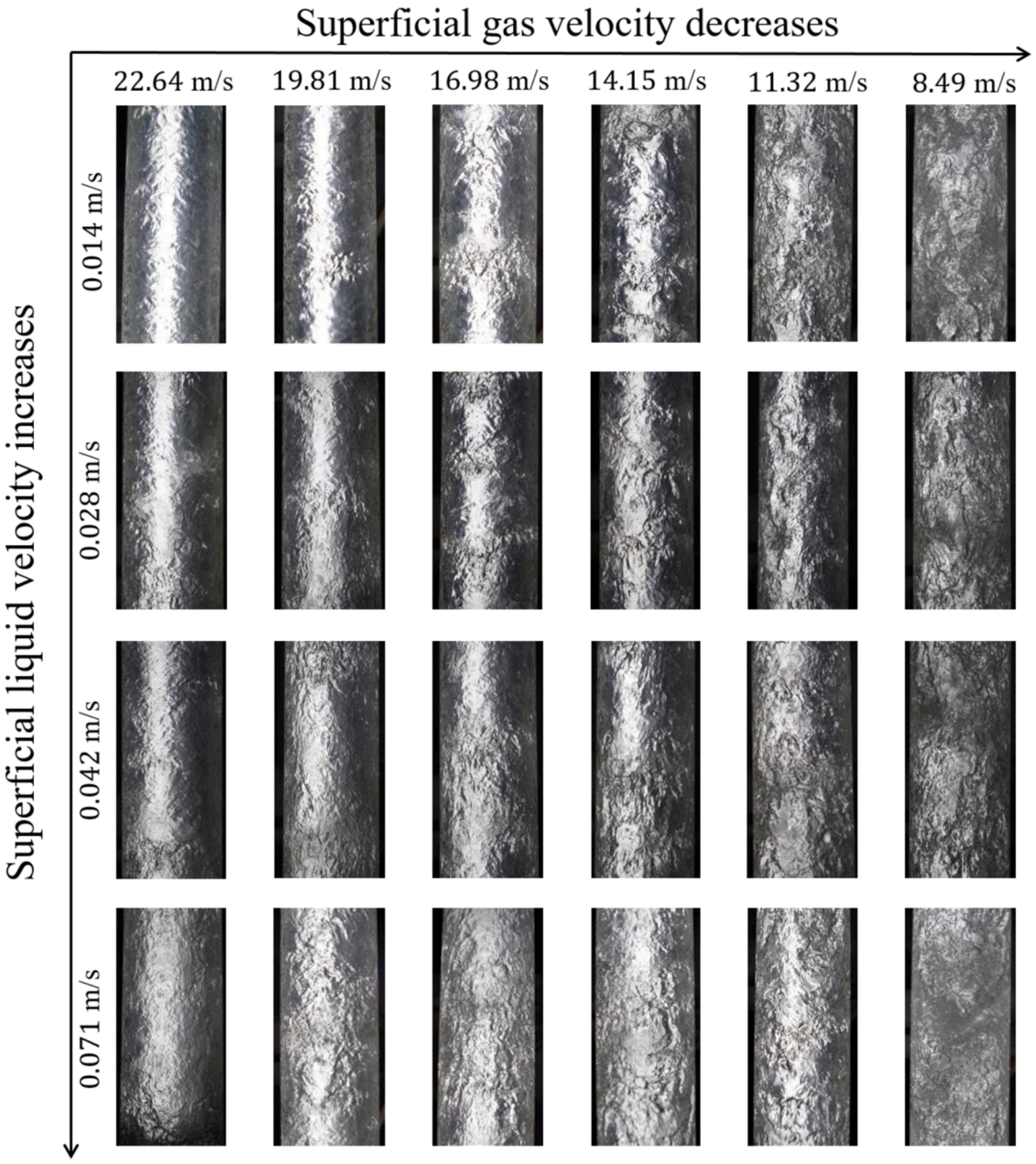

Fig. 6. Decreasing superficial gas velocity at each superficial liquid velocity.

modified angle correlations and friction factors. The Liu et al. (2018) model was developed based on the zero wall shear stress condition, and used the Belfroid et al. (2008) angle correction in inclined pipes. The Turner et al. (1969) model is the most widely used droplet reversal model. The Belfroid et al. (2008) model modified the Turner et al. (1969) model by introducing an angle correction term.

The comparison of the experimental and predicted data for different pipe angles is shown in Fig. 8. The horizontal axis represents the measured experimental data, while the vertical axis represents the estimated critical gas velocity. If the predicted data matches the measured values, then the symbols approach the diagonal. Specifically, Table 2 and Fig. 9 present the average absolute relative errors for each model. The absolute relative error (ε) is calculated by $\varepsilon(\%) = \frac{1}{N}\sum_{i=1}^{N}|K_p - K_m|/K_m \times 100$, where N is the number of data, K_p is the predicted value, and K_m is the measured value.

When pipes are vertical ($\beta = 90^{\circ}$), Figs. 8(a) and 9(a) show that Barnea (1986) and S. Luo et al. (2014) overestimate the critical gas velocities considerably and their errors are 40.00% and 31.03% respectively. J. Li et al. (2014) and Liu et al. (2018) over-predict the value slightly in vertical pipes. Some results of Belfroid et al. (2008) and Turner et al. (1969) are underestimated. The errors by J. Li et al. (2014), Liu et al. (2018), Turner et al. (1969), and Belfroid et al. (2008) range from 10% to 20%. The simplified model, unified model, and Shekhar et al. (2017) model have great predictions because their predicted results are close to the diagonal and errors are less than 10%. In general, the simplified model in Section 2.2 has the best prediction in vertical pipes with the smallest error of 5.28%.

At pipe angles ranging from 60° to 80°, it can be seen that the S. Luo et al. (2014) model has significant overestimation with the largest error of 31.03%. The Turner et al. (1969) model underestimated the results with an error of 27.95%. The models by Barnea (1986), Liu et al. (2018), and Belfroid et al. (2008) have slight discrepancies with the measured results and their errors are between 10% and 20%. The simplified model, the unified model, J. Li et al. (2014) model, and Shekhar et al.

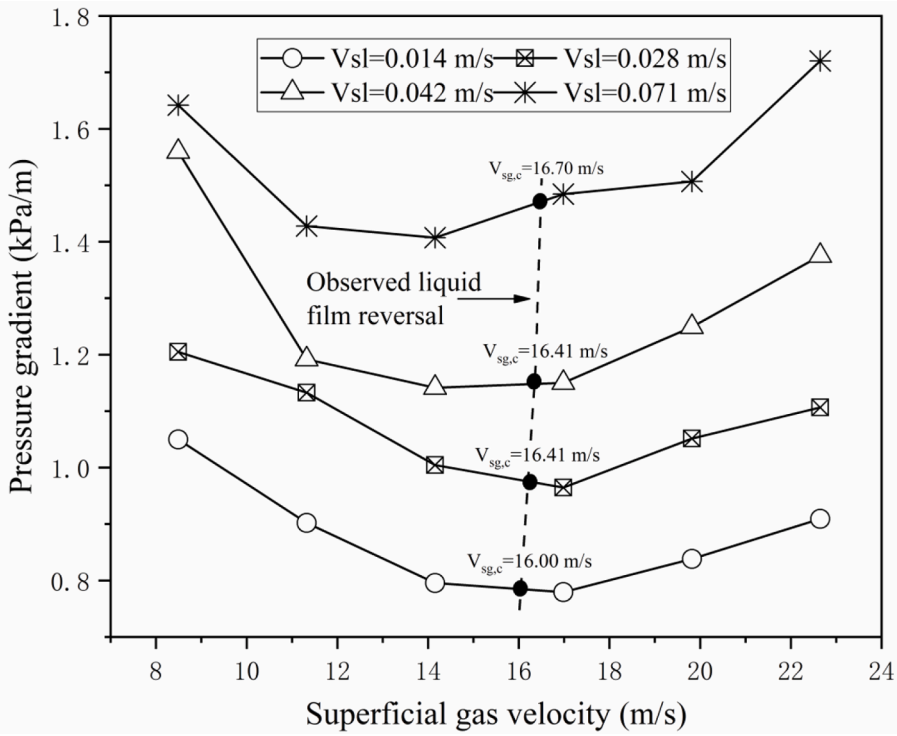

Fig. 7. Measured pressure gradient in the current experiment.

Table 1
Experimental data for model evaluation.

Datasets	data number	Pipe diameter (mm)	Liquid phase	Gas phase	Pipe angle (°)	Superficial liquid velocity (m/s)
Fan et al. (2018)	15	0.0762	Water	Air	2–20	0.01–0.1
Skopich et al. (2015)	4	0.051; 0.102	Water	Air	90	0.1; 0.05
Rastogi and Fan et al. (2020)	18	0.1524	Water	Air	1–90	0.001–0.01
Liu et al. (2018)	12	0.03	Water	Air	15–90	0.01–0.05
Guner et al. (2015)	12	0.0763	Water	Air	45–90	0.01–0.1
Alsaadi et al. (2015)	20	0.0762	Water	Air	2–30	0.01–0.1
Current work	4	0.05	Water	Air	90	0.014–0.071

(2017) model exhibit good predictions with errors of less than 10%. The error of Shekhar et al. (2017) model is the smallest of 5.94%. It should be noted that the simplified model only shows a slightly larger error (6.22%) than the Shekhar et al. (2017) model.

When the pipe inclination ranged from 30° to 50°, the majority of predictions in Turner et al. (1969), Barnea (1986), S. Luo et al. (2014), and Belfroid et al. (2017) are underestimated. The Turner et al. (1969) model has the largest of 35.13%. Some results of S. Luo et al. (2014) and Liu et al. (2018) are over-predicted. The simplified model, the unified model, and the Shekhar et al. (2017) model yield good predictions with errors of less than 10%. And, the error of the simplified model error is the smallest of 5.85%.

At pipe angles less than 20°, the Barnea (1986), J. Li et al. (2014), Turner et al. (1969) and Belfroid et al. (2008) models underestimate the critical gas velocities significantly. The errors of the four models exceed 20%. The errors of other models are similar and between 13% and 15%. The S. Luo et al. (2014) model has the smallest error of 12.94%. The errors of the proposed simplified model and unified model are 13.84% and 14.12%, respectively. It can be seen that some predictions of the proposed two models are underestimated, as shown in Fig. 8(d). We found that these under-predictions happened when the pipe diameter is large (0.1524) and the angle is near horizontal (1° and 5°), where the flow regime may be stratified flow (Ratosgi and Fan, 2020). In the stratified flow, the film thickness at the pipe bottom may be thicker, and the real critical gas velocity may be higher than the expected results by the proposed models. Other models by S. Luo et al. (2014), Shekhar et al. (2017), and Liu et al. (2018) also present a similar phenomenon. Although there is a limitation in large and near horizontal pipes, the proposed two models are acceptable because the errors are less than 15%.

The total average absolute relative errors for each model are displayed in Fig. 9(b). In general, it can be seen that the simplified model is superior to other models with the smallest error of 10.18%. Additionally, Shekhar et al.'s (2017) model also performs well with an error of 10.23%. The error of the unified model is 11.56%, which is slightly larger than the simplified model and Shekhar et al. (2017) model. The errors of Liu et al. (2018) and J. Li et al. (2014) models are smaller than 20%. The errors of Barnea (1986), S. Luo et al. (2014), Turner et al. (1969), and Belfroid et al. (2008) models exceed 20%. The Barnea (1986) model shows the largest error of 35.00%.

3.2.2. *Evaluation with the field data in the literature*

The field data from published literature was collected to evaluate different models. As presented in Table 3, the tubing inner diameter in the field data ranged from 0.04 m to 0.187 m. The pipe inclined from 27° to 90° The in-situ pressure was from 0.29 to 34 MPa. These parameters cover most cases in natural gas wells. Turner et al. (1969) reported the gas rates in 90 gas wells, including 31 loaded wells, 53 unloaded wells,

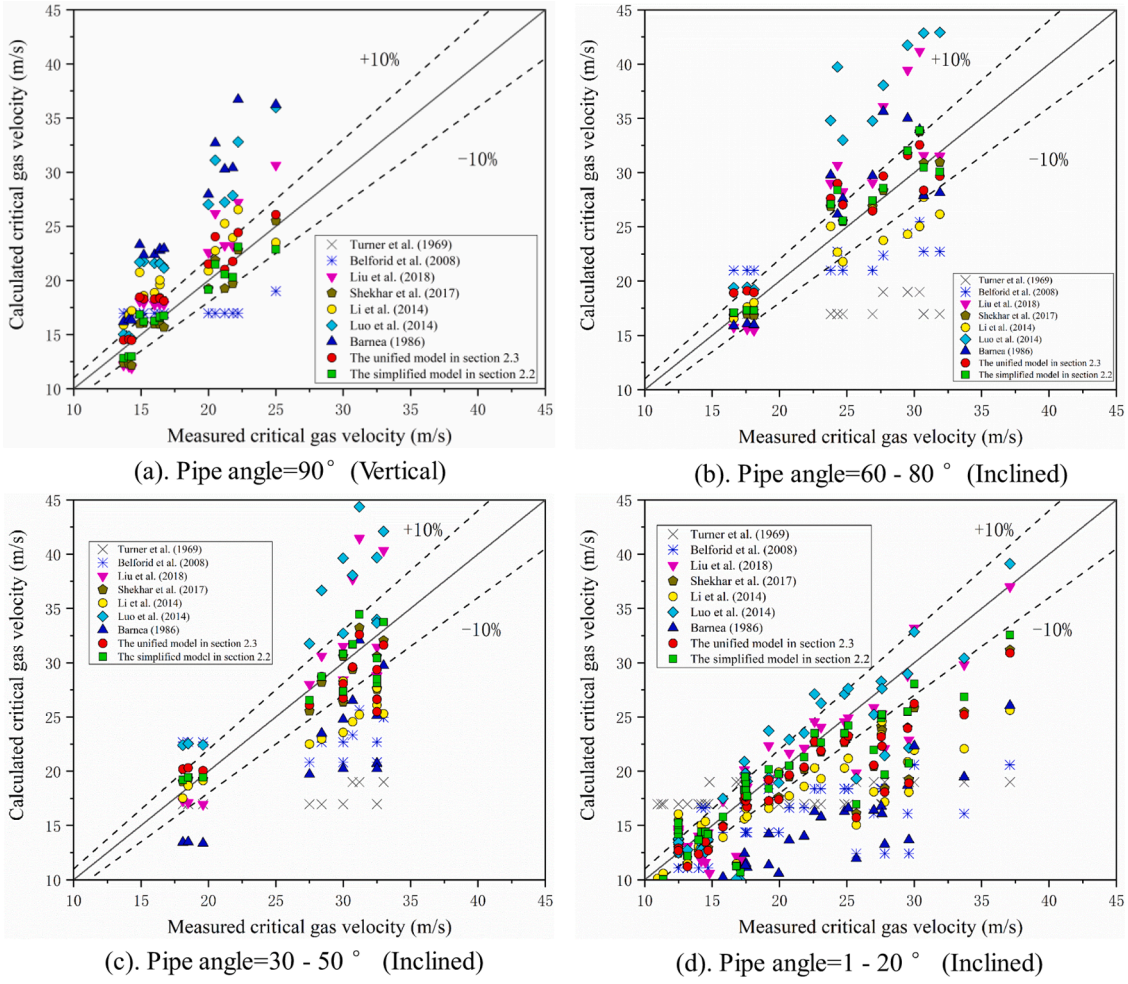

Fig. 8. Model evaluation with the experimental data and different pipe angles.

Table 2
Average absolute relative errors of different models.

Angle (°)	Average absolute relative errors (%) The simplified model	The iterative model	Barnea (1986)	S. Luo et al. (2014)	J. Li et al. (2014)	Shekhar et al. (2017)	Liu et al. (2018)	Turner et al. (1969)	Belfroid et al. (2008)
90	5.28	9.45	40.00	31.03	18.21	6.43	14.61	14.98	15.02
60–80	6.22	9.12	13.29	34.32	8.56	5.94	17.10	27.95	18.70
30–50	5.85	8.36	23.32	20.75	14.31	6.39	11.50	35.13	25.48
1–20	14.12	13.84	42.50	12.94	20.32	13.74	13.12	34.35	25.70

and 6 near-loaded wells. Coleman et al. (1991) and Veeken et al. (2009) reported 56 and 67 loaded gas wells, respectively. It should be noted that the observed gas rates in Coleman et al. (1991) and Veeken et al. (2009) were close to the inception of liquid loading; hence, the gas wells in the two publications are near-loaded in fact.

The predicted critical gas velocities from the proposed two models, as well as the published models, were compared with the observed gas rates in the field. There are two parameters for model evaluation. The first parameter is the accuracy of the predicted liquid-loading status, which is calculated by $\text{Accuracy}\ (\%) = \frac{\text{Correctly predicted number of gas wells}}{\text{Total number of gas wells}} \times 100$. If the predicted critical gas velocity is larger than the observed gas rate, then the gas well should be loaded, and vice versa. Another parameter is the absolute relative error between the predicted result with the observed value in near-loaded wells. For a good prediction, the accuracy should be high and the relative error should be small. It should be noted that the predicted critical gas velocities were transformed to the production rates at the wellhead.

Fig. 10 displays the accuracy of predicted liquid-loading status for each model. It can be seen that the accuracy of the simplified model and the unified model is better than published models in Turner et al's (1969) data, as shown in Fig. 10(a). But, in the datasets from Coleman et al. (1991) and Veeken et al. (2009), it is obvious that the models by Barnea (1986), S. Luo et al. (2014), and J. Li et al. (2014) have better accuracy. And, the total accuracy presents in Fig. 10(d) shows that the accuracy of Luo et al.'s (S. 2014) model is the best of 91.30%.

In Fig. 10, it seems that the proposed simplified model and unified model do not have great performance in liquid loading wells. However, it should be noted that the accuracy in Fig. 10 only describes the ability to predict the liquid-loading status, and this accuracy cannot present the precision of predicting critical gas velocity. For instance, as long as the predicted critical gas velocity is larger than the measured value in loaded wells, the forecast is correct. We found that the good accuracy in models by Barnea (1986), S. Luo et al. (2014), and J. Li et al. (2014)

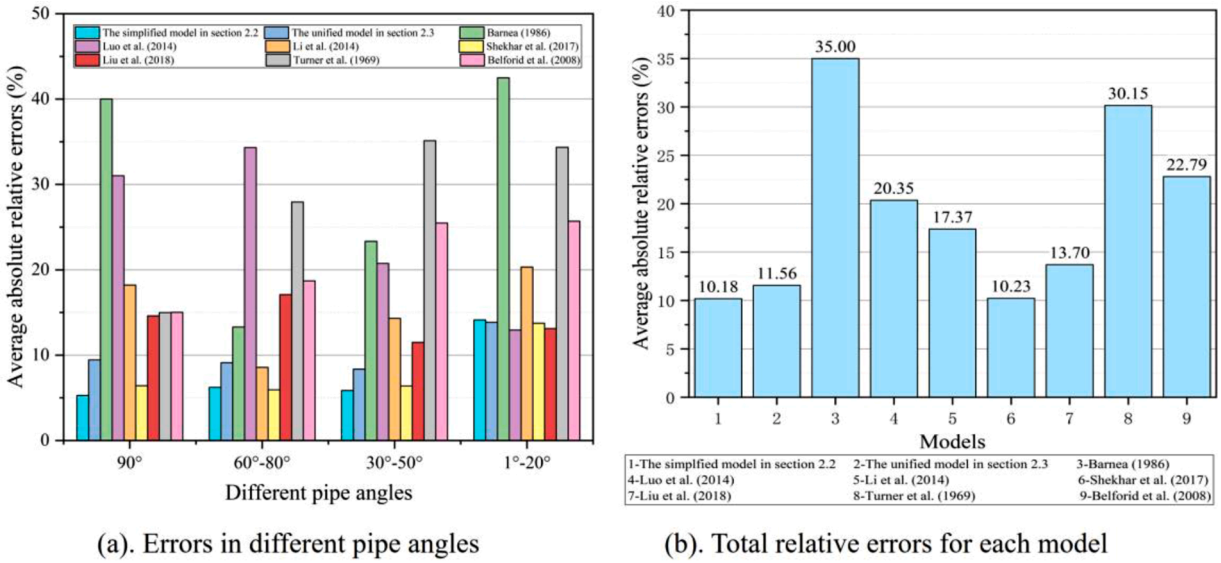

Fig. 9. Average absolute relative errors for each model (Laboratory data).

Table 3
Field data for model evaluation.

Sources	Tubing inner diameter (m)	Average pipe angle (°)	Wellhead pressure (Mpa)	Number of gas wells	Remarks
Turner et al. (1969)	0.04 - 0.187	90	0.74 – 34	90	There are 90 available wells, including 31 loaded wells, 53 unloaded wells, and 6 near loaded wells.
Coleman et al. (1991)	0.062	90	0.29 – 2.17	56	The 56 wells are near loaded
Veeken et al. (2009)	0.044 – 0.154	27 - 90	0.4 – 11.1	67	The 67 wells are near loaded

owes to the overprediction of critical gas velocities in most cases. Therefore, Fig. 10 cannot impede the performance of the proposed models in predicting critical gas velocity. And, by introducing a safety factor of 1.18 into the proposed models, the accuracy can be improved to approximately 90%.

The errors between the predicted gas velocities and observed gas rates for each model are presented in Fig. 11. It can be seen that the simplified model has the best prediction in the datasets from Turner et al. (1969) and Coleman et al. (1991). In Veeken et al.'s (2009) dataset, the Belfroid et al. (2008) has the smallest error of 22.23%. But it should be noted that Belfroid et al. (2008) model's accuracy for liquid-loading status in Fig. 10(c) is relatively small (13.43%); hence, this model's capacity in forecasting liquid-loading status should be improved.

In general, as shown in Fig. 11(d), the simplified model has the smallest total error of 27.03%, outperforming other models. The models by Shekhar et al. (2017) and Belfroid et al. (2008) also exhibit good prediction with the total errors slightly larger than the simplified model. The unified model has a total relative error of 34.26%, which is also acceptable in engineering considering that the conditions in the wellbore are complex.

3.3. Evaluation results

The evaluation results show that the simplified model has the smallest errors of 10.18% in laboratory experiments and 27.03% in field tests, meaning that it is superior to the unified model and published models to accurately predict the critical gas velocity. Hence, the simplified model in Section 2 is recommended to predict liquid film reversal. Besides, it should be noted that a safety factor of 1.18 should be added to the model to forecast the liquid-loading status.

The total errors of the unified model are 11.56% in the laboratory and 34.26% in the field, which is greater than the majority of published models, except the Shekhar et al. (2017) model. The Shekhar et al. (2017) model exhibits better predictions than the unified model, but worse results than the simplified model.

This section evaluates the accuracy of the proposed and published models comprehensively. In the following two sections, detailed model comparisons are presented to discuss the features and the contributions of the proposed models.

4. Model comparisons for the simplified model

4.1. In vertical pipes

4.1.1. Two critical criteria of film reversal

The simplified model used the zero wall shear as the critical condition of film reversal, while the unified model and the published models by Barnea (1986), S. Luo et al. (2014), J. Li et al. (2014), and Shekhar et al. (2017) utilized the stability analysis as the critical criterion. Hence, it is worth discussing the differences between the two criteria of zero wall shear and stability analysis.

The mechanism of stability analysis has been illustrated by Taitel et al. (1982). As shown in Fig. 12, the solid black lines represent the interfacial shear required to lift liquid film flow upward, which were plotted using Eq. (16). Taitel et al. (1981) clarified that the minimum point in the black lines denotes the critical status when the liquid film begins to lose stability. Hence, the connecting line of the minimum interfacial point corresponds to the critical condition of stability analysis, as plotted by the dashed blue line in Fig. 12. The zero wall shear condition has been presented in Fig. 2. By Eq. (5), Fig. 12 plots the relationship between the dimensionless interfacial shear and film thickness when the wall shear is zero, as shown by the dashed red line.

Fig. 12 displays that the dashed red line is very close to the dashed

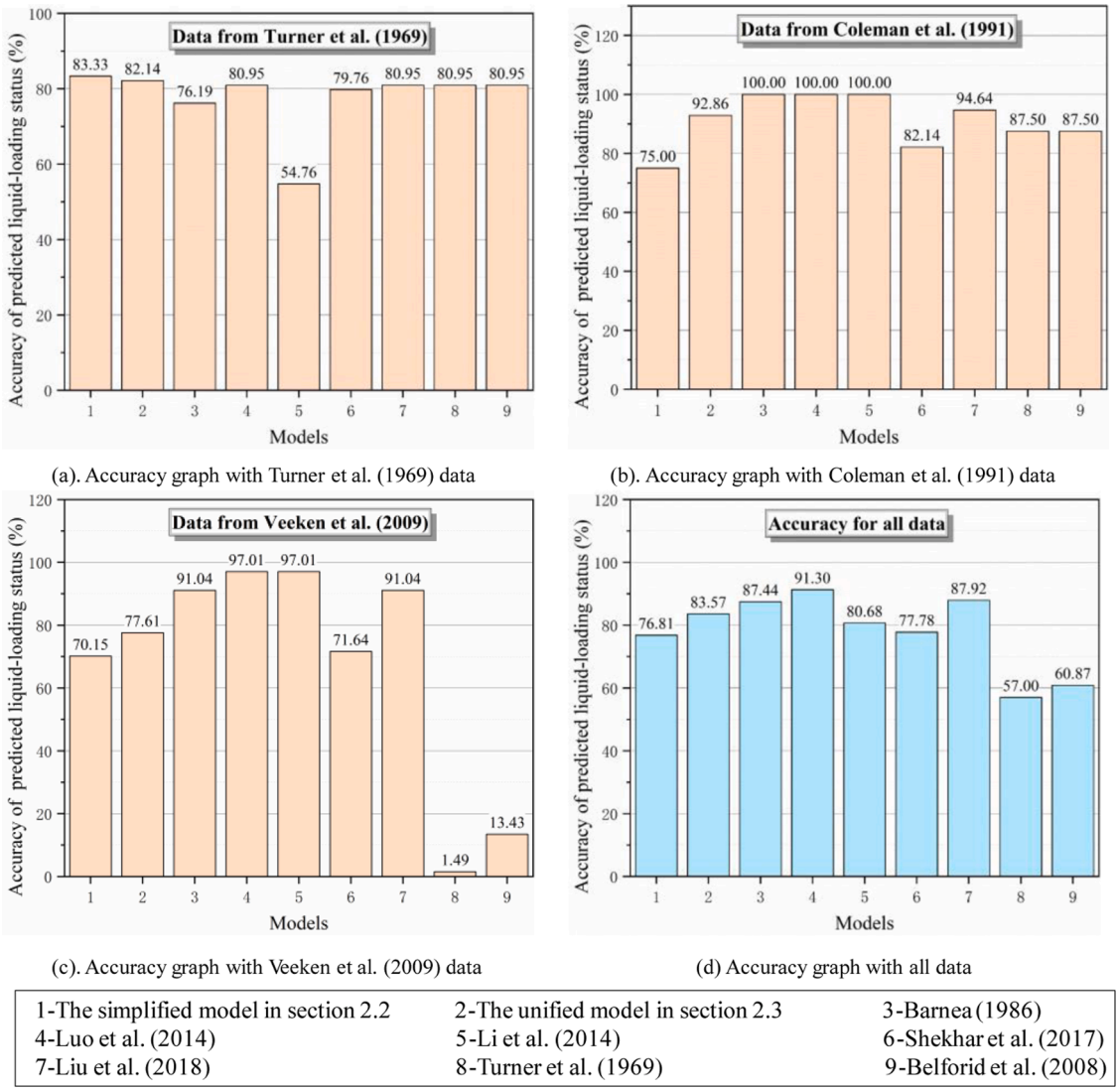

(a). Accuracy graph with Turner et al. (1969) data

(b). Accuracy graph with Coleman et al. (1991) data

(c). Accuracy graph with Veeken et al. (2009) data

(d) Accuracy graph with all data

Fig. 10. Accuracy of predicted liquid-loading status for each model.

blue line. Error analysis shows that the maximum relative errors between the two dashed lines are less than 2%, which means that when the interfacial shear is minimal and the liquid film begins to lose stability, the wall shear stress approaches zero. This phenomenon shows that both critical criteria (stability analysis and zero wall shear condition) can be applied to predict the onset of film reversal. This can explain why the film reversal models based on the two different critical conditions have been found to be feasible in previous studies.

4.1.2. *Ignoring of higher-order terms in formulations*

As presented in Section 2.2, the simplified model ignores the higher-order terms in Eqs. (2) and (5) to obtain the analytical expressions. Fig. 13 presents the influences of ignoring the higher-order terms in vertical pipes. Fig. 13(a) is the graph representing the predicted results versus the measured value in vertical pipes from Table 1. The red symbols denote the results without ignoring the higher-order terms, which are calculated using Eqs. (2) and (5). The green symbols are the results ignoring the higher-order terms, which are obtained by Eqs. (9) and (10). It can be seen from Fig. 13(a) that ignoring higher-order terms leads to over-predictions of the critical gas velocities. Fig. 13(b) shows that the results by ignoring the higher-order terms cause a relative error of 13.46%, which is larger than the error without ignoring higher-order terms (11.59%). Hence, neglecting the higher-order terms in the simplified model results in over-prediction and larger errors.

4.1.3. *Ignoring of droplet entrainment fraction*

Compared with the unified model, the simplified model ignores the droplet entrainment. To discuss the influences of droplet entrainment, two droplet entrainment fraction correlations by Wallis (1968) and Barbosa et al. (2002) were employed in the simplified model.

Fig. 14(a) shows that, when the droplet entrainment fraction is ignored, the predicted symbols are above the diagonal, denoting that the results without droplet entrainment are overestimated. When the droplet entrainment is taken into account, the predicted results are smaller than the values of ignoring the droplet entrainment. The predicted symbols with Wallis's (1968) correlation are closer to the diagonal than the results with Barbosa et al.'s (2002) correlation. Specifically, the relative errors are displayed in Fig. 14(b). It can be seen that the error without the droplet entrainment is 13.46%. When the entrainment fraction is considered, the relative errors with Wallis's (1968) correlation and Barbosa et al.'s (2002) correlation are 10.43% and 12.20%, respectively. Hence, ignoring the droplet entrainment in the simplified model leads to overestimation and larger discrepancy.

Combing with the results in Section 4.1.2, it can be seen that, because of the simplifications of higher-order terms and droplet entrainment fraction, the simplified model can result in over-predicted and

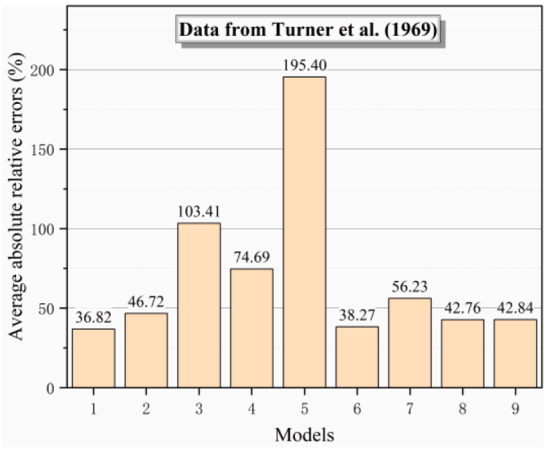

(a). Relative error graph with Turner et al. (1969) data

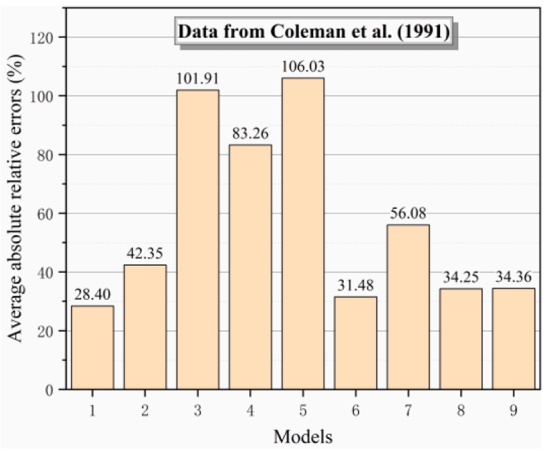

(b). Relative error graph with Coleman et al. (1991) data

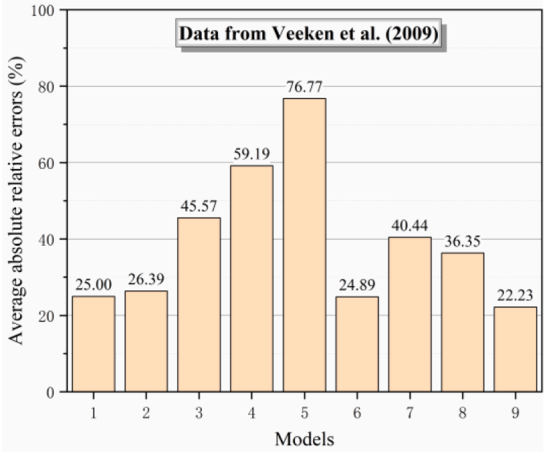

(c). Relative error graph with Veeken et al. (2009) data

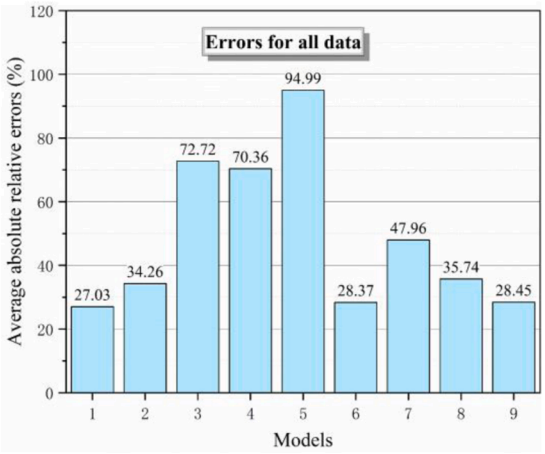

(d). Relative error graph with all data

1-The simplified model in section 2.2	2-The unified model in section 2.3	3-Barnea (1986)
4-Luo et al. (2014)	5-Li et al. (2014)	6-Shekhar et al. (2017)
7-Liu et al. (2018)	8-Turner et al. (1969)	9-Belforid et al. (2008)

Fig. 11. Average absolute relative errors for each model (field data).

inaccurate results. This problem can be addressed by introducing the angle modification term, which will be presented in the next Section 4.2.

4.2. *In inclined pipes*

Compared with the models by Belfroid et al. (2008) and Liu et al. (2018), the simplified model utilizes a modified angle term in Belfroid et al. (2008), which improves the simplified model's performance in vertical and inclined pipes. Fig. 15 shows the influences of different angle correction terms on the critical gas velocities.

Fig. 15 displays that the measured critical gas velocities increase firstly with the decrease of pipe angle. When pipe angle approaches about 40°, the critical gas velocity reaches the maximum. Then, the critical gas rate decreases with the decreasing pipe angle. The solid red lines are the results without the angle correction, and it can be seen that the estimation is constant and independent of the pipe angle. When Belfroid et al.'s (2008) angle term is introduced, the prediction shows a similar tendency with the experimental results, as plotted by the dashed black lines in Fig. 15. But, it can be seen that the results by Belfroid et al.'s (2008) term are overestimated in the range from 90° to 50° This overestimation may be explained by two reasons. The first reason is the simplification of higher-order terms and droplet entrainment fraction, as illustrated in Sections 4.1.2 and 4.1.3. Another reason may be the intrinsic undercities of Belfroid et al.'s (2008) term. Therefore, as shown in Eq. (15), Belfroid et al.'s (2008) term was modified to optimize its performance and prevent the over-prediction from 90° to 50° The predictions by the modified Belfroid relation (i.e. the simplified model) are plotted by the dashed pink lines in Fig. 15. It is obvious that results with the modified angle term in this work are closer to the measured data.

Specifically, the relative errors by different angle correction terms are presented in Fig. 16. It can be seen that the prediction by the modified angle term in the present work is superior to the previous angle term because of the smaller relative errors, especially when the angle is larger than 20°, as shown in Fig. 16(a). The total relative errors in Fig. 16 (b) also illustrate that the modified angle correction term is better. Compared with the prediction with the original Belfroid et al.'s (2008) angle term, the simplified model with the modified angle term can reduce the total relative error to 10.18%.

4.3. *Contributions of the simplified model*

The main contribution of the simplified model is that it provides a practical approach to predict the critical gas velocity of film reversal conveniently and accurately. This simplified model is expressed by an analytical solution so that users can obtain the critical gas velocity directly. As shown in Section 3.3, the simplified model is more accurate than other models with the evidence of model evaluation.

However, based on the model comparisons, it should be emphasized

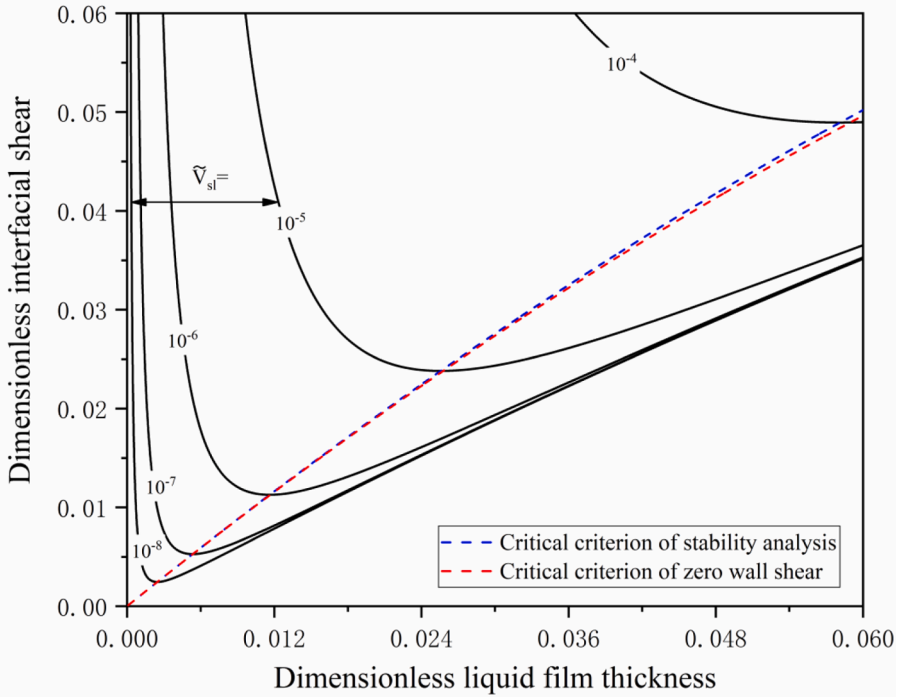

Fig. 12. Comparison between two critical criteria (stability analysis and zero wall shear).

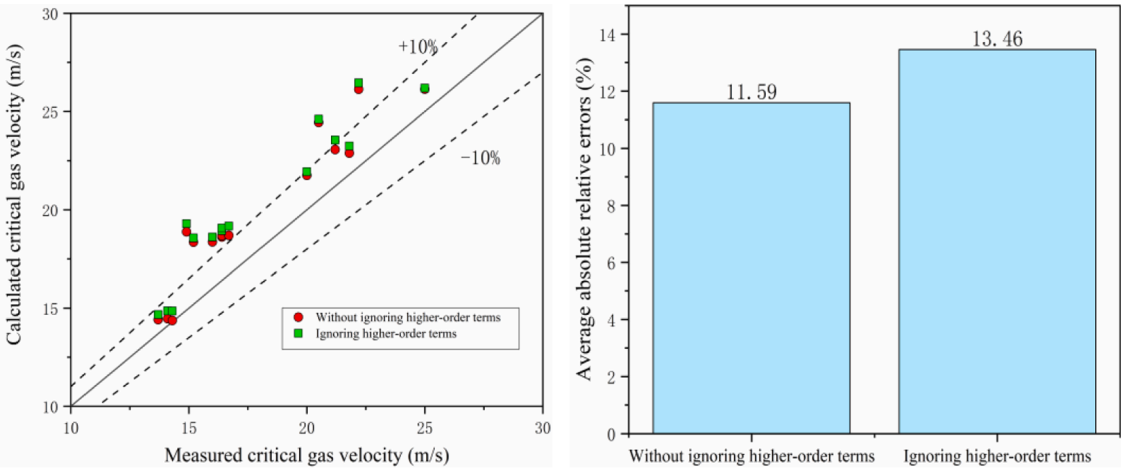

(a). Measured data v.s. predicted data (b). Average absolute relative errors

Fig. 13. The influences of ignoring the high-order terms in vertical pipes.

that the simplified model is a trade-off in simplification and accuracy. To reach the goal of simple form, the simplified model ignores the higher-order terms and droplet entrainment, leading to overestimation and inaccuracy compared with the measured results. On the other hand, to achieve high accuracy, Belfroid et al's (2008) angle correction term is modified to prevent the overestimation in vertical and inclined pipes. Hence, it can be seen that, because of these characteristics, the simplified model may not be rigorous to clarify such a complicated phenomenon of film reversal. As a result, to understand the underlying mechanism of film reversal further, the unified model, which is more rigorous in theory, will be discussed in the next section.

5. Model comparisons for the unified model

5.1. In vertical pipes

In vertical pipes, we mainly compared the Barnea (1986) model with the unified model because other models by S. Luo et al. (2014), J. Li et al. (2014), and Shekhar et al. (2017) are modified from the Barnea (1986) model by introducing angle correction correlation in inclined pipes.

The model evaluation in Section 3.2 has shown that the Barnea (1986) model leads to significant over-prediction, while the unified model is better than the Barnea (1986) model. This could be attributed to the two improvements in the unified model: the interior liquid film viscosity and the droplet entrainment fraction.

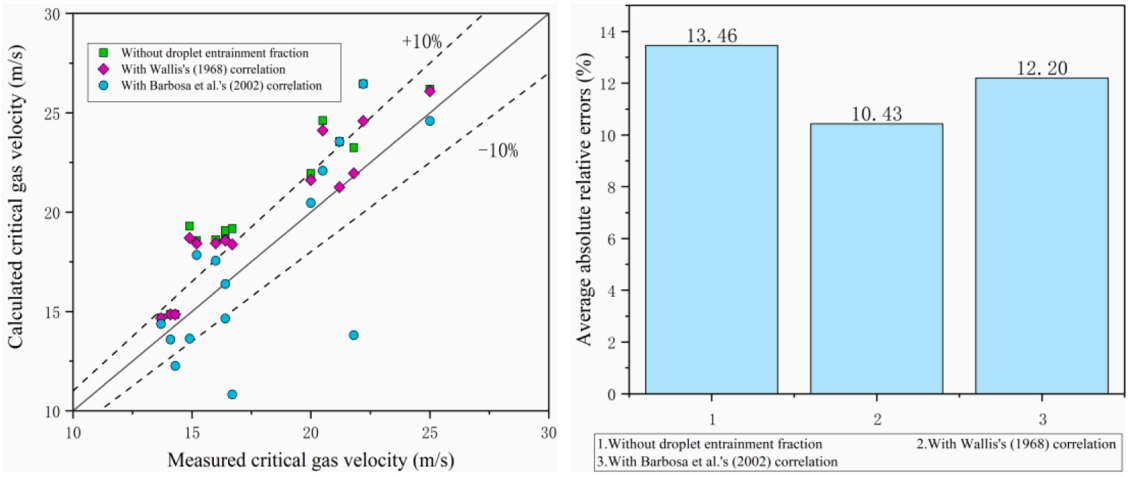

(a). Measured data v.s. predicted data (b). Average absolute relative errors

Fig. 14. The influences by ignoring droplet entrainment in vertical pipes (the simplified model).

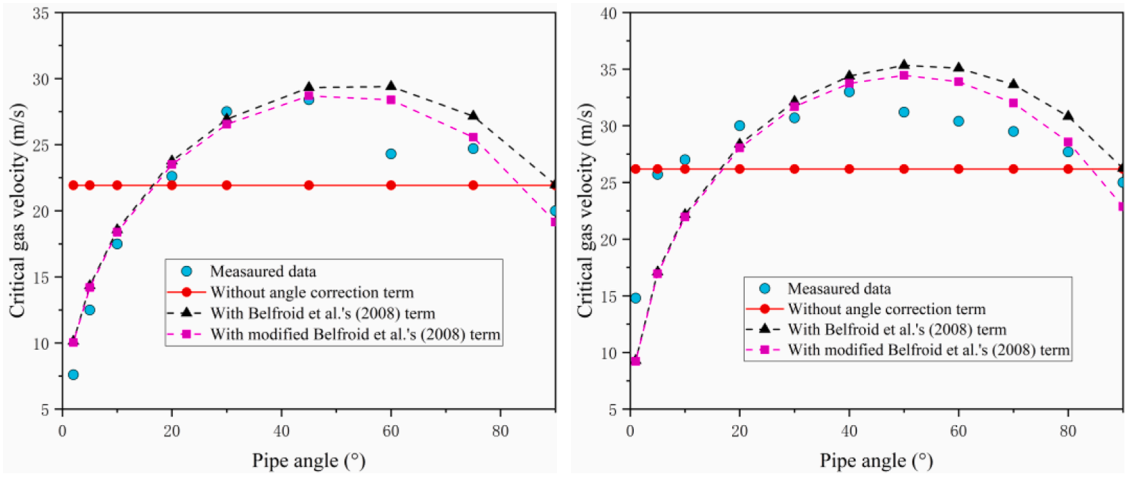

(a). Pipe ID= 76.2 mm, Vsl=0.01 m/s (Guner et al., 2015; Alssadi et al., 2015)

(b). Pipe ID= 154 mm, Vsl=0.001 m/s (Rastogi and Fan, 2020)

Fig. 15. Critical gas velocity with different angle terms in inclined pipes.

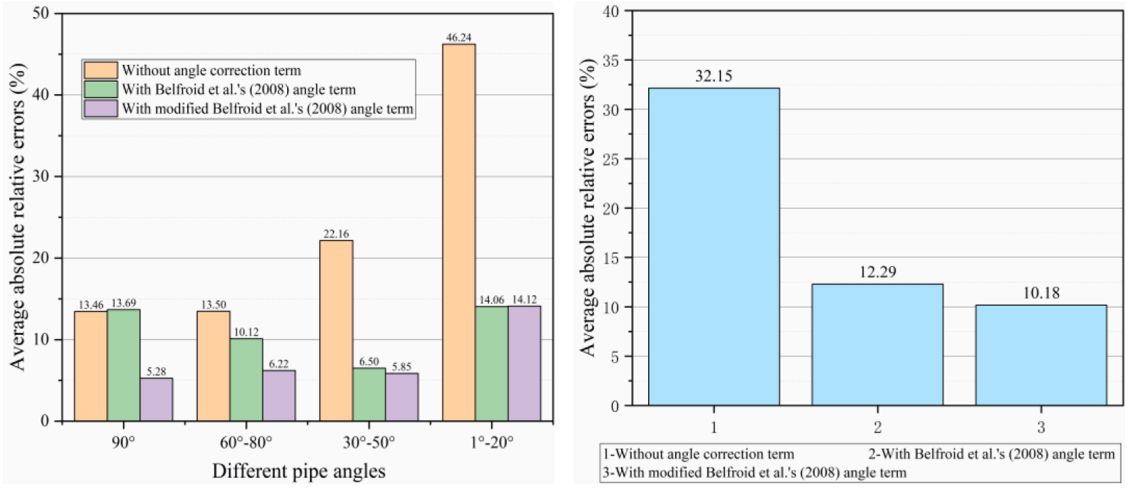

(a). Average absolute relative errors in different angles (b). Total Average absolute relative errors

Fig. 16. Average absolute relative errors for different angle correction terms.

$$\widetilde{\tau}_i = \underbrace{\frac{(1-2\widetilde{\delta_u})}{2\left(\widetilde{\delta_u}-\widetilde{\delta_u}^2\right)^2}\widetilde{V_{sl}}}_{\text{Term-1: caused by the wall shear } (\tau_w)} + \underbrace{\sin\beta\,(1-2\widetilde{\delta_u})\left\{\frac{1}{4}+\frac{(1-2\widetilde{\delta_u})^2\left[(1-2\widetilde{\delta_u})^2\ln\frac{1}{1-2\widetilde{\delta_u}}-2\left(\widetilde{\delta_u}-\widetilde{\delta_u}^2\right)\right]}{16\left(\widetilde{\delta_u}-\widetilde{\delta_u}^2\right)^2}\right\}}_{\text{Term-2: caused by the viscosity } (\tau_v) \text{ and gravity } (g)}$$

(b). The expression of the interfacial shear in Eq. (16)

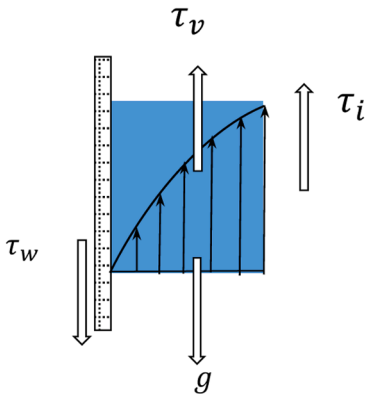

(a). Liquid film's force balance

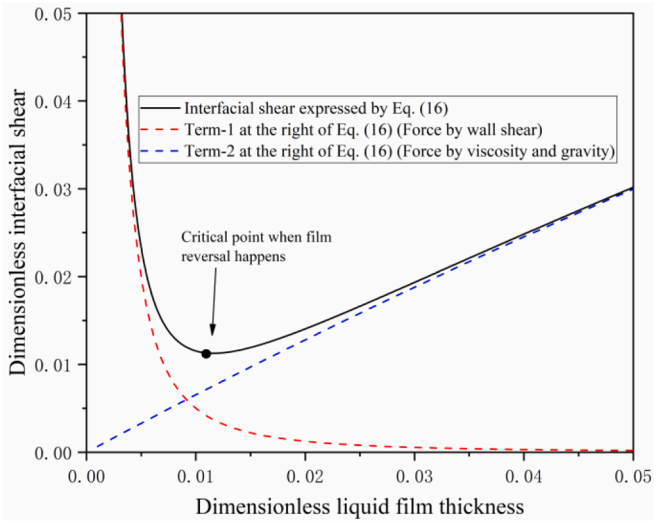

(c). Graph of the interfacial shear ($\widetilde{V_{Sl}} = 10^{-6}, \beta = 90°$)

Fig. 17. Analysis of the interfacial shear in annular flow.

Table 4
Comparison of the interfacial shear in the unified model and Barnea (1986) model.

Model	Interfacial shear = Term-1 (caused by wall shear) + Term-2 (caused by liquid viscosity and gravity)	
	Term-1	Term-2
The unified model (Eq. (16))	$\frac{(1-2\widetilde{\delta_u})}{2(\widetilde{\delta_u}-\widetilde{\delta_u}^2)^2}\widetilde{V_{SL}}$	$\sin\beta(1-2\widetilde{\delta_u})\left\{\frac{1}{4}+\frac{(1-2\widetilde{\delta_u})^2\left[(1-2\widetilde{\delta_u})^2\ln\frac{1}{1-2\widetilde{\delta_u}}-2(\widetilde{\delta_u}-\widetilde{\delta_u}^2)\right]}{16(\widetilde{\delta_u}-\widetilde{\delta_u}^2)^2}\right\}$
Barnea model (1986)	$\frac{(1-2\widetilde{\delta_u})}{2(\widetilde{\delta_u}-\widetilde{\delta_u}^2)^2}\widetilde{V_{SL}}$	$\sin\beta(1-2\widetilde{\delta_u})(\widetilde{\delta_u}-\widetilde{\delta_u}^2)$

5.1.1. *Significance of the liquid film viscosity*

To understand the significance of the liquid film viscosity, it is pertinent to briefly describe the interfacial shear in annular flow at first.

As plotted in Fig. 17(a), there are four forces in the liquid film: the interfacial shear between the gas and liquid phases, the force by the interior liquid viscosity, the force of gravity, and the wall shear stress. Therefore, the interfacial shear should be the balance of the gravity, viscosity force, and wall shear stress. Section 2.3 presents that Eq. (16) is the expression of the interfacial shear in annular flow. As shown in Fig. 17(b), Eq. (16) can be divided into two terms: Term-1 is caused by the wall shear, and Term-2 is caused by liquid film viscosity and gravity. Fig. 17(c) plots Eq. (16), as well as the two terms at the right of Eq. (16).

In Fig. 17(c), it can be seen that Term-1 decreases with the increase of film thickness, as shown by the dashed red line. This can be explained by that, with the increase of film thickness, the liquid phase's flow area increases accordingly; then the real liquid velocity decreases, leading to the decrease of the wall shear. The dashed blue line in Fig. 17(c) shows that Term-2 increases with the increasing film thickness. This is caused by that thicker film results in more gravity. The two opposite functions contribute to the total interfacial shear, as depicted by the solid black line in Fig. 17(c). It shows that, when the film thickness is small, the total interfacial shear is dominated by Term-1. The interfacial shear decreased significantly with the increase in film thickness. After reaching the minimum value, the total interfacial shear began to increase because the rapid increase in gravity (Term-2) dominates the interfacial shear. Taitel et al. (1982) reported that the minimum point of the interfacial shear is a critical condition for film reversal, as shown by the black point in Fig. 17(c).

Then, the interfacial shear expressions in the unified model and Barnea (1986) model are compared, as shown in Table 4. It can be seen that Term-1 is the same in the two models, while Term-2 in the Barnea (1986) model is simpler than that in Eq. (16). This difference is caused by the assumption of the rigid liquid film by Barnea (1986), which means that the interior viscosity in the liquid film is ignored. In contrast, the unified model considers the interior viscosity, so Term-2 in the unified model is different from it in the Barnea (1986) model.

Fig. 18 displays the differences of the interfacial shear in the two models. It can be seen that Term-2 in the Barnea (1986) model is larger than that in the unified model. This indicates that because the upward force induced by the liquid viscosity is ignored, the interfacial shear must be larger to balance the gravity of the liquid film. Therefore, the interfacial shear stress required to keep the liquid film flowing steadily in the Barnea (1986) model is larger than that in the unified model, as indicated by the black points in Fig. 18. Accordingly, a higher gas velocity is required for a larger interfacial shear, leading to the overestimation. This explains the over-prediction in Barnea (1986) model theoretically.

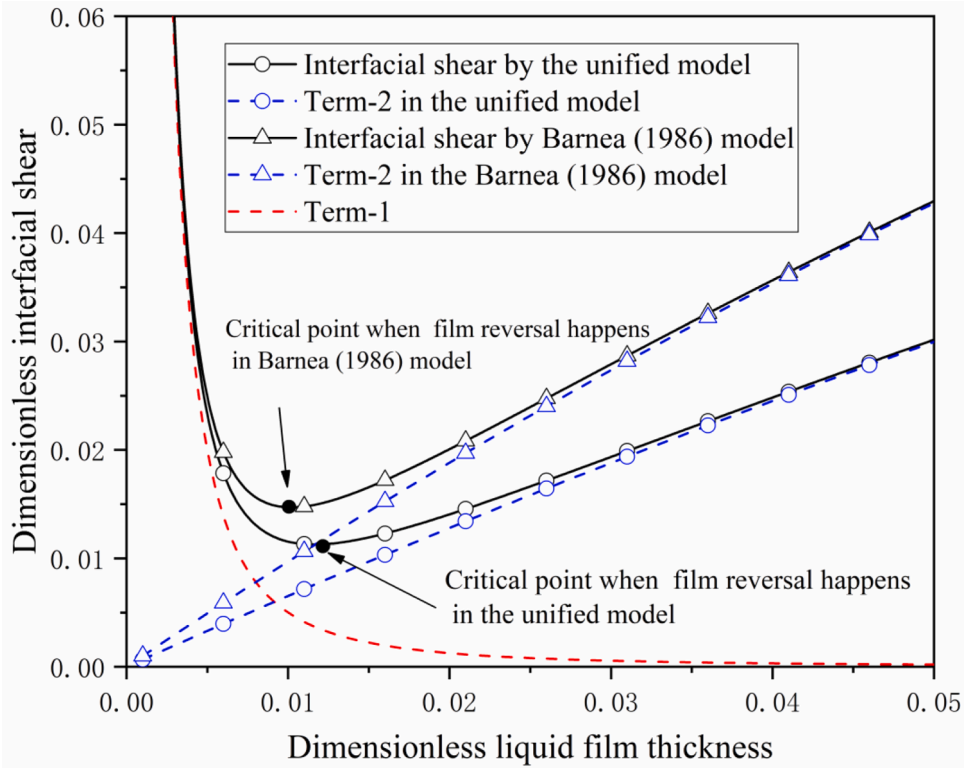

Fig. 18. Comparison of interfacial shear stress ($\widetilde{V_{Sl}} = 10^{-6}$, $\beta = 90°$).

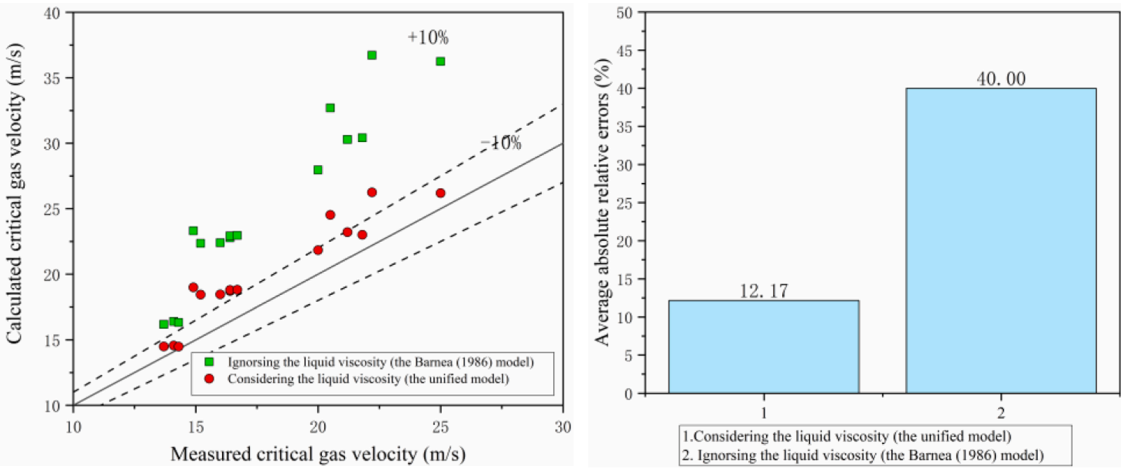

(a). Measured data v.s. predicted data (b). Average absolute relative errors

Fig. 19. The influences by ignoring liquid film viscosity in vertical pipes.

Fig. 19 shows the influence of the liquid film viscosity on the critical gas velocity. Fig. 19(a) shows that the Barnea (1986) model overestimates the gas velocity considerably compared with the measured results. In contrast, the predictions considering the liquid viscosity are closer to the diagonal. Fig. 19(b) presents that the relative error in the Barnea (1986) model is 40.00%. By taking the liquid viscosity into account, the relative error can be decreased to 12.17%, which is a significant optimization. Therefore, the unified model is superior to Barnea (1986) model by considering the liquid film viscosity.

5.1.2. *Significance of the droplet entrainment fraction*

Although the liquid film viscosity is considered in Section 5.1.1, it can be seen that the results still have some overestimation compared with the measured results. This overestimation can be mitigated further by taking the droplet entrainment fraction into account.

Fig. 20 shows the influences by introducing the droplet entrainment in the unified model. For comparison, the results by Barbosa et al. (2002) were presented here. The red symbols in Fig. 20(a) are the results of the unified model ignoring the droplet entrainment fraction. The blue symbols are the results by introducing the correlation of Barbosa et al. (2002). The green symbols are predicted by introducing the entrainment correlation of Wallis (1986). It can be seen that the predictions with entrainment fraction are smaller than the results without entrainment fraction. The predictions with Wallis's (1986) correlation are closer to the diagonal than the results with Barbosa et al.'s (2002) correlation. Fig. 20(b) illustrates that the relative error with the Wallis correlation is the smallest of 9.45%, which is smaller than the error without droplet entrainment fraction (12.17%). The error by the Barbosa et al. (2002)

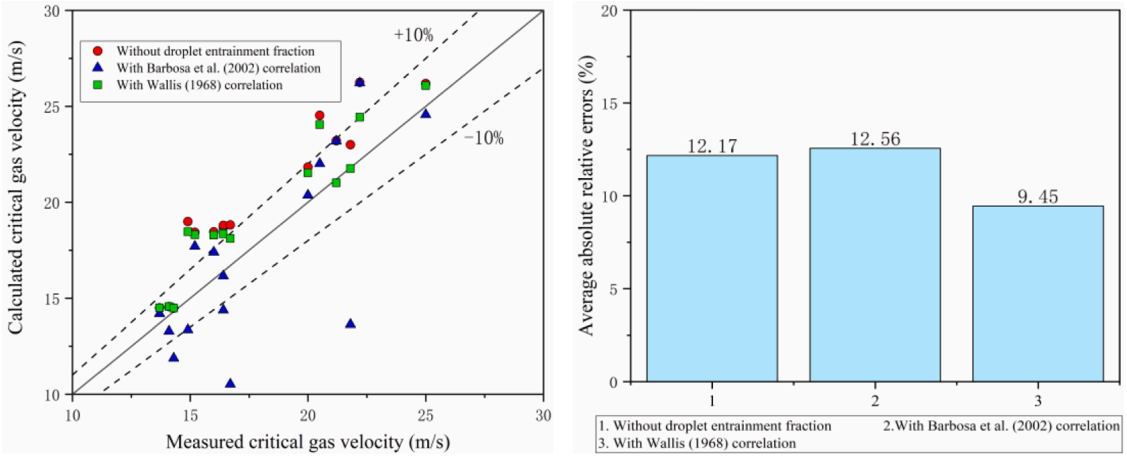

(a). Measured data v.s. predicted data (b). Average absolute relative errors

Fig. 20. The significance of droplet entrainment in vertical pipes (the unified model).

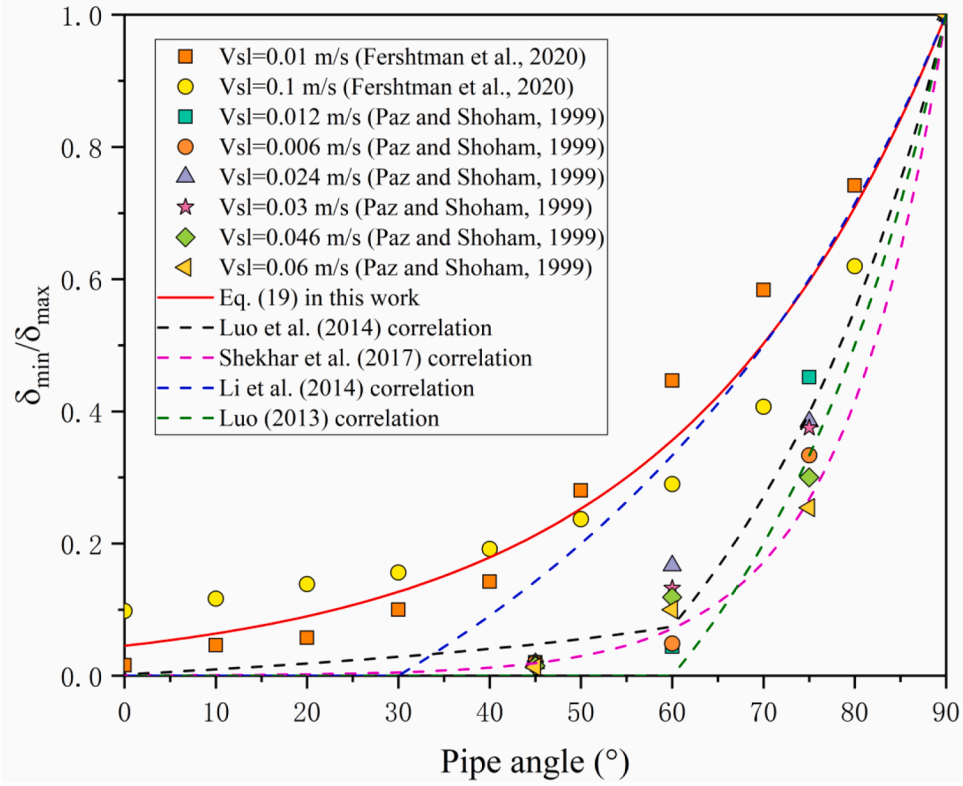

Fig. 21. δ_{min} /δ_{max} varying with pipe angle.

correlation is the largest of 12.56%. Therefore, although the Barbosa et al. (2002) correlation can mitigate the overestimation, it could lead to larger errors. By using the entrainment fraction correlation of Walis (1968), the predictions are better and the error can be reduced to less than 10%.

5.2. *In inclined pipes*

5.2.1. *Film thickness correlations*

The non-uniform film thickness distribution in inclined pipes is an important factor in the film reversal model. Compared with the models by S. Luo et al. (2014), J. Li et al. (2014), and Shekhar et al. (2017), the unified model adopted the new empirical correlation δ_{min} /δ_{max} (Eq. (19)) to modify the uniform film thickness into a non-uniform film thickness. To fit Eq. (19), the experimental data of Freshtman et al. (A. 2020) was used. Freshtman et al. (A. 2020) measured the circumferential film thickness in pipes with an inner diameter of 24 mm, superficial liquid velocities of 0.1 m/s and 0.01 m/s, and superficial gas velocity of 20 m/s, respectively. The pipe angles in their experiment ranged from 0° to 90° Because the liquid velocity is low in most cases of film reversal, the non-uniform film thickness was assumed to be independent of the liquid velocity. Therefore, the average values of the measured data at different liquid velocities were used to fit the empirical correlation (Eq. (19)), as shown by the solid red line in Fig. 21. The average absolute error of the new correlation is 7.70%.

In S. Luo et al. (2014), Shekhar et al. (2017), and J. Li et al. (2014),

Table 5
Angle correlation for non-uniform thickness distribution.

Authors	Correlations	Remarks
Luo (2013)	$\frac{\delta_{min}}{\delta_{max}} = \begin{cases} \frac{1-\frac{(90-\beta)}{30}}{1+\frac{(90-\beta)}{30}} & 60 < \beta \le 90 \\ & 0\ \beta \le 60 \end{cases}$	Proposed from Paz and Shoham experiment (1999)
S. Luo et al. (2014)	$\frac{\delta_{min}}{\delta_{max}} = \begin{cases} \frac{1-0.0287(90-\beta)}{1+0.0287(90-\beta)} & 60 < \beta \le 90 \\ \frac{1-0.55(90-\beta)^{-0.868}(90-\beta)}{1+0.55(90-\beta)^{-0.868}(90-\beta)} & \beta \le 60 \end{cases}$	Proposed from Paz and Shoham experiment (1999)
Shekhar et al. (2017)	$\frac{\delta_{min}}{\delta_{max}} = \exp[-8.80 \times 10^{-2}(90-\beta)]$	Proposed from Paz and Shoham experiment (1999)
J. Li et al. (2014)	$\frac{\delta_{min}}{\delta_{max}} = \begin{cases} \frac{1-\frac{(90-\beta)}{60}}{1+\frac{(90-\beta)}{60}} & 30 < \beta \le 90 \\ & 0\ \beta \le 30 \end{cases}$	Corrected from Luo correlation (2013)
Current work (Eq. (19))	$\frac{\delta_{min}}{\delta_{max}} = \exp[-3.44 \times 10^{-2}(90-\beta)]$	Proposed from Fershtman et al. experiment (A. 2020)

the measured data from Paz and Shoham (1999) was used to fit the correlation of the film thickness. Fig. 21 compares the measured data from Freshtman et al. (A. 2020) and Paz and Shoham (1999). Compared with Freshtman et al.'s (A. 2020) work, Paz and Shoham (1999) conducted the experiments in pipes with an inner diameter of 51 mm and angles at 45, 60, 75, and 90°. Fig. 21 shows that the $\delta_{min}/\delta_{max}$ in Freshtman et al. (A. 2020) is larger than it in Paz and Shoham (1999), especially when pipe angle ranges from 40° to 80° However, it remains unclear why the film thickness distributions in Freshtman et al. (A. 2020) and Paz and Shoham (1999) are different. Investigating the interior structure of annular flow in inclined pipes is a challenging job that is beyond the scope of this paper. If additional experimental works on non-uniform film thickness in different pipe diameters are conducted in the future, then the mechanism of the film distribution could be revealed. In this work, the objective is to clarify the angle modification method and predict the critical gas velocity in inclined pipes. Hence, a reasonable approach is to evaluate the capacity of different film thickness correlations using the measured critical gas velocity.

We collected film correlations of $\delta_{min}/\delta_{max}$ fitted by Luo et al. (2013), S. Luo et al. (2014), J. Li et al. (2014), and Shekhar et al. (2017), as listed in Table 5. The previous four correlations are developed by Paz and Shoham's (1999) experimental data. It should be noted that Li et al.'s (J. 2014) correlation was modified from Luo et al. (2013) model. The correlations in Table 5 are plotted in Fig. 21. It can be seen that the correlations of Luo et al. (2013), S. Luo et al. (2014), and Shekhar et al. (2017) have similar results, which are smaller than the Eq. (19) in this work. The results of J. Li et al. (2014) are fairly close to the Eq. (19) when the pipe angle is between 60° and 90° However, the results are underestimated compared with Eq. (19) when the pipe angle is less than 60°

To evaluate the different angle correlations, the different relations in Table 5 were introduced into the unified model to calculate the critical gas velocities. Fig. 22 presents the estimated results and the measured value in different pipe angles. Figs. 22(a) and (b) show that the predicted critical gas velocities with Luo (2013), S. Luo et al. (2014), and Shekhar et al. (2017) are similar. Compared with the measured critical gas velocities, the estimated results with the three relations were

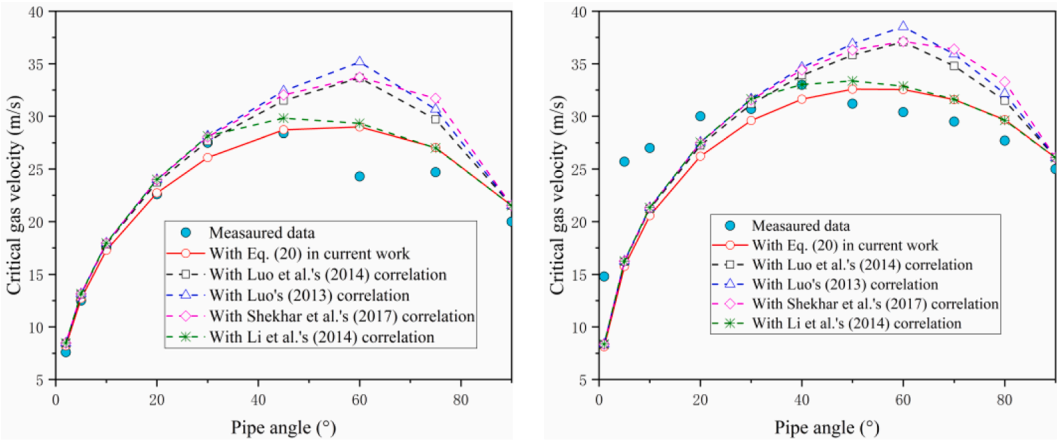

(a). Pipe ID= 76.2 mm, Vsl=0.01 m/s (Guner et al., 2015; Alssadi et al., 2015)

(b). Pipe ID= 154 mm, Vsl=0.001 m/s (Rastogi and Fan, 2020)

Fig. 22. Critical gas velocity with different angle correlations at different pipe angles.

Table 6
Different correlations of interfacial friction factors.

Models	Correlations of interfacial friction factor	Authors of the correlations	Remarks
Barnea (1986)	$f_i = 0.005(1 + 300\tilde{\delta_u})$	Wallis (1969)	Based on fully developed annular flow
S. Luo et al. (2014)	$f_i = 0.005\left(1 + 300\left[\left(1, + \frac{1,750,0}{,Re_{,G}}\right)\tilde{\delta_u} - 0.0015\right]\right)$	L.B. Fore et al. (2000)	Based on fully developed annular flow
Shekhar et al. (2017)	$f_i = 0.005\{1 + 340[1 + \cos(90-\beta)]\tilde{\delta_u}\}$	Shekhar et al. (2017)	Modified from Wallis's (1969) correlation
J. Li et al. (2014)	$\begin{cases} \frac{f_i}{f_g} = 1 + 15\tilde{\delta_u}^{0.5}\left(\frac{V_{sg}}{V_{sg,t}}\right) for\ V_{sg} \ge V_{sg,t} \\ \frac{f_i}{f_g} = 1\ for\ V_{sg} < V_{sg,t} \end{cases}$	Andritsos and Hanratty (1987)	Based on fully developed horizontal stratified flow
The unified model	$f_i = 0.005(1 + 300\tilde{\delta_u})$	Wallis (1969)	Based on fully developed annular flow

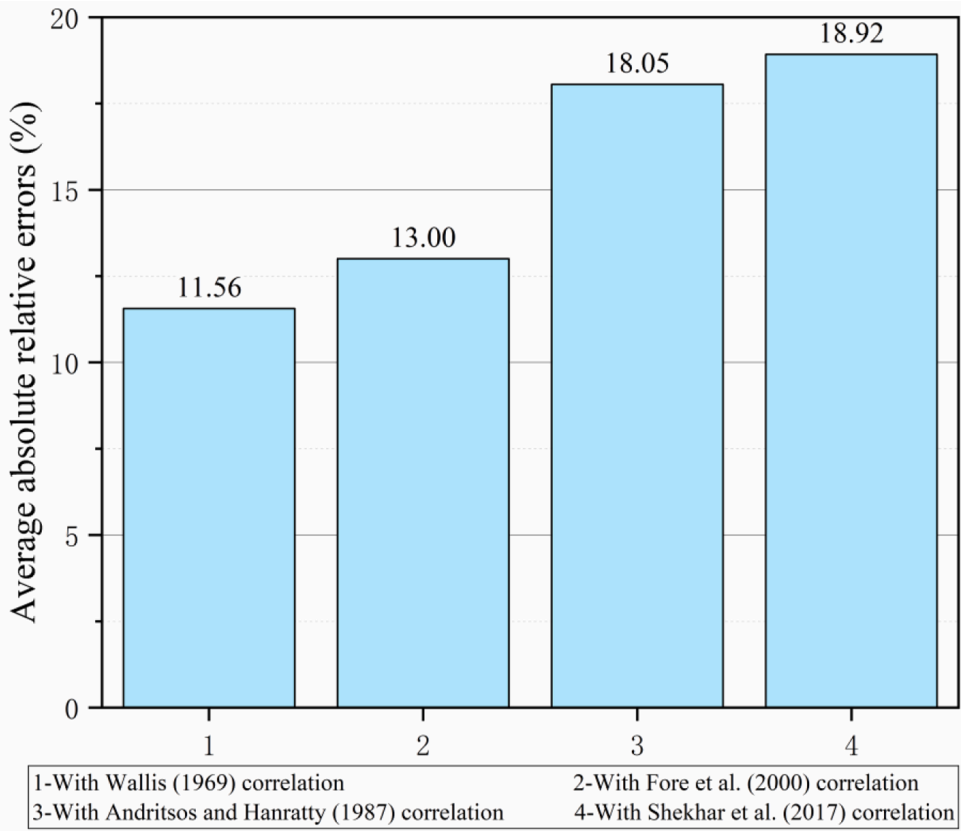

Fig. 23. The average absolute relative errors with different interfacial friction factors.

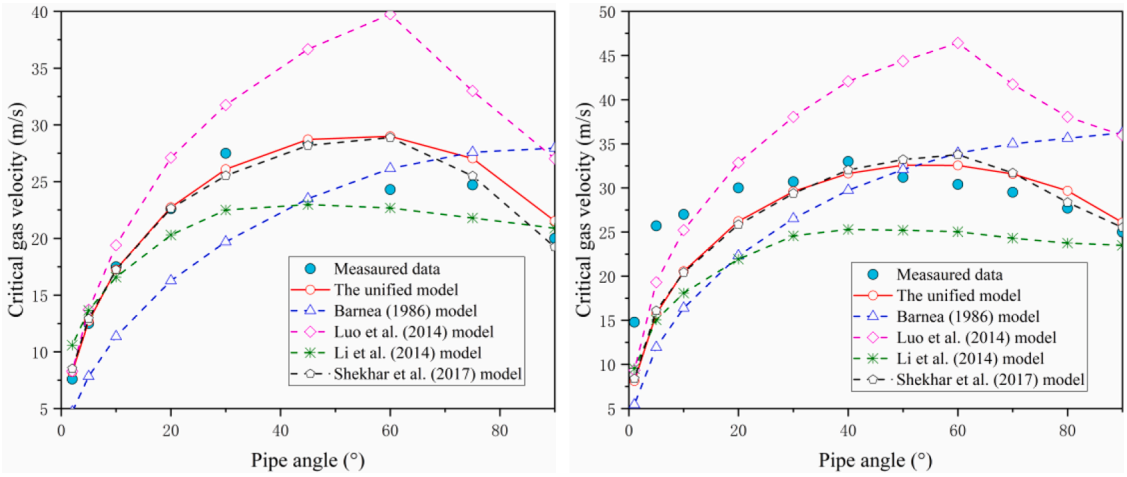

(a). Pipe ID= 76.2 mm, Vsl=0.01 m/s (Guner et al., 2015; Alssadi et al., 2015)

(b). Pipe ID= 154 mm, Vsl=0.001 m/s (Rastogi and Fan, 2020)

Fig. 24. Critical gas velocity by different models in inclined pipes.

overestimated, especially in the angle range between 50° and 90° The results predicted with the relation in the present work and J. Li et al. (2014) are similar in the angle range of 50° to 90° Both relations provide accurate predictions compared with the experimental data. However, it should be noted that the empirical relation of J. Li et al. (2014) was modified from the Luo (2013) relation directly; hence, it may lack the support of experimental evidence. When the pipe angle is less than 40°, it can be seen that the results with all the relations are similar and correspond with the experimental data, except for the case of a large diameter pipe. Fig. 22(b) shows that all correlations underestimated the critical gas velocity when the pipe angle was less than 20° As discussed in Section 3.2.1, the liquid film in large inner diameter and near horizontal pipes would be stratified, leading to a higher critical gas velocity. However, because there are few measured data on film thickness in large diameter and near horizontal pipes, it is difficult to obtain a reliable relation for that case. This limitation is expected to be addressed in the future if additional measurements of film thickness in large diameter pipes are conducted. Summarily, compared with previous correlations, Eq. (19) in the current work performed better for a wider range of pipe diameters and pipe angles, especially in the angle range from 50° to 90°

5.2.2. Interfacial friction factor

The interfacial friction factor is a crucial parameter in film reversal models. Different interfacial friction factors used in various models are listed in Table 6. Wallis's (1969) correlation was initially proposed and had the simplest form. Fore. et al.'s (2000) correlation improved Wallis's (1969) correlation by introducing the gas Reynolds number (Re_G). Fore et al.'s (L.B. 2000) correlation has an uncertainty of 25%. Andritsos and Hanratty's (1987) correlation is proposed for fully developed horizontal stratified flow. The solution method and descriptions of this friction factor can be referred to Andritsos and Hanratty's (1987) and J. Li et al. (2014). Shekhar et al. (2017) modified Wallis's (1969) correlation by introducing the pipe angle into account; but, the details regarding Shekhar et al. (2017) factor's applicability and accuracy were not reported. It should be noted that these correlations were originated from fully developed annular flow or stratified flow. There are few investigations about the interfacial friction factor for film reversal, especially in inclined pipes. Therefore, the correlations in Table 6 are introduced to the unified model to evaluate their performance for predicting critical gas velocities.

Fig. 23 presents the average absolute relative errors with different interfacial friction factors using the measured data from Table 1. It can be seen that the results with Wallis's (1969) correlation have the smallest error of 11.56%. Fore et al.'s (L.B. 2000) correlation results in a larger error of 13.00%. The correlations of Andritsos and Hanratty (1987) and Shekhar et al. (2017) lead to errors of 18.05% and 18.92%, respectively. Hence, Wallis's (1969) correlation is used in the unified model because it shows better performance to predict the film reversal.

5.2.3. Critical gas velocity in inclined pipes

Fig. 24 compares the unified model with previous models by Barnea (1986), S. Luo et al. (2014), J. Li et al. (2014), and Shekhar et al. (2017) at different pipe angles. It can be seen that the Barnea (1986) model cannot capture the tendency of critical gas velocity varying with angles, because it ignores the non-uniform distribution of the film thickness. Although the S. Luo et al. (2014) model can capture the tendency of the pipe angle, it is overestimated significantly. The J. Li et al. (2014) model is underestimated in the range from 20° to 90° The unified model and Shekhar et al. (2017) model have great predictions for the measured data and can capture the tendency of the gas velocity varying with pipe angles.

Specifically, the model evaluations in Section 3 have presented that the accuracy of Shekhar et al. (2017) model is slightly better than the unified model. We found that Shekhar et al. (2017) model's high accuracy attributes to the modified interfacial friction factor, which remedies the inaccuracy in vertical and inclined pipes. As aforementioned, the Shekhar et al. (2017) model is based on Barnea's (1986) model, which has the feature of overestimation in vertical pipes, as discussed in Section 5.1. In inclined pipes, Shekhar et al.'s (2017) correlation of film thickness modification also leads to overestimation when pipe angle is between 50° and 90°, as presented in Fig. 22. Then, Shekhar et al. (2017) modified the friction factor of Wallis (1969) by introducing the pipe angle, and results showed great performance when compared with measured data. Therefore, Shekhar et al.'s (2017) work showed that fitting a suitable friction factor for film reversal is a feasible approach to improve the model's performance. But, as presented in Fig. 23, the modified friction factor by Shekhar et al. (2017) is not reliable for the unified model. Hence, although Shekhar et al.'s (2017) model exhibits good predictions, the underlying mechanism of the interfacial friction factor of film reversal is still unclear, especially in inclined pipes. This problem is expected to be studied in detail in the future.

5.3. Contributions of the unified model

In summary, the principal contribution of the unified model is that it improves the film reversal model rigorously in vertical and inclined pipes. Compared with published film reversal models, the unified model considers the liquid film viscosity and droplet entrainment. In inclined pipes, the unified model adopts a new film thickness correlation. With these improvements, the unified model can reach the total prediction error of 11.56% in the laboratory, outperforming the majority of previous models.

It should be claimed that, although the development of the unified model is rigorous in mechanism, some limitations may impede the accuracy of the unified model. Some input parameters in the unified model have not been investigated comprehensively. The mechanisms of droplet entrainment fraction, interfacial friction factor, and film thickness distributions in vertical and inclined pipes at the condition of film reversal are unclear. And, these parameters are difficult to be measured and calculated currently, making it difficult to use the unified model. These problems are expected to be addressed in the future with more theoretical and experimental researches on film reversal.

6. Conclusions and suggestions

The present work proposed two film reversal models and conducted laboratory experiments for model evaluation. The proposed model was compared with those of previous studies to discuss the contributions of the proposed models. The findings of this work will be helpful in improving the film reversal mechanism and reducing the risk of liquid loading in gas wells.

A simplified model of film reversal with an analytical solution was proposed based on the zero wall shear condition. Dimensionless graphs were developed to easily obtain the critical gas velocity at different flow conditions. Compared with the measured critical gas velocities, the simplified model had great prediction results with total relative errors of 10.18% in the laboratory and 27.03% in the field, outperforming the unified model and previous models. When predicting the liquid-loading status, a safety factor of 1.18 is suggested in the simplified model. Because of the merits of simple form and high accuracy, the simplified model is recommended to predict the critical gas velocity of film reversal for practical use. It should be claimed that the simplified model is not rigorous in the mechanism because of its simplifications. This gap can be filled by the unified model.

Based on the stability analysis of annular flow, a rigorous unified film reversal model with an iterative solution was proposed in vertical and inclined pipes. The model evaluation showed that the total errors of the unified model were 11.56% in the laboratory and 34.26% in the field. The unified model was superior to published models by taking the interior viscosity of the liquid film into account, which considerably alleviated the overestimation in published models and reduced the total relative error in vertical pipes from 40.00% to 12.17%. Further, by considering the droplet entrainment fraction, the predicted results of the unified model were better and the total error can be reduced to 9.45% in vertical pipes. In inclined pipes, the unified model adopted a new empirical correlation for the modification of the non-uniform film thickness distribution. Compared with previous correlations, the new empirical relation had better performance with pipe angles ranging between 50° and 90°, whereas previous empirical relations overestimated the critical gas velocity. These results showed the improvements of the unified model compared with published models. But, because of the rigorous mechanism, the unified model was difficult to be used widely.

In general, although there are some limitations, the contributions in the proposed two models complement each other practically and theoretically. The simplified model can predict film reversal conveniently and accurately, while the unified model is helpful to understand the mechanism of film reversal because it describes the film reversal rigorously.

CRediT authorship contribution statement

Li-song Wang: Conceptualization, Methodology, Validation,

Writing – original draft. **Shuo Liu:** Conceptualization, Resources, Investigation. **Lin-tong Hou:** Data curation, Investigation, Visualization. **Meng Yang:** Visualization, Investigation, Resources. **Jian Zhang:** Supervision, Investigation. **Jing-yu Xu:** Conceptualization, Supervision, Project administration, Funding acquisition.

Declaration of Competing Interest

The authors declare that they have no known competing financial interests or personal relationships that could have appeared to influence the work reported in this paper.

Acknowledgments

This work present here is financially supported by National Natural Science Foundation of China (no. 51779243) and the Strategic Priority Research Program of the Chinese Academy of Science (Grant no: XDB22030101).

Appendix A. - Derivation of the simplified model

Under the axial symmetry condition, the momentum equation of the liquid film around the pipe wall is given as

$$\frac{\mu_l}{\rho_l}\frac{1}{r}\frac{\partial}{\partial r}\left(r\frac{\partial V_l}{\partial r}\right)-\frac{1}{\rho_l}\frac{dP}{dz}-g\sin\beta=0 \tag{A-1}$$

where μ_l is the liquid viscosity (Pa·s), ρ_l is the liquid density (kg/m^3), r is the radial distance from the center of the pipe (m), V_l is the liquid velocity (m/s), $\frac{dP}{dz}$ is the pressure gradient (Pa/m), g is the acceleration of gravity (m/s^2), and β is the pipe angle (degree, 90° is vertical).

By integrating Eq. (A-1) twice, the velocity distribution of the liquid film is given by Eq. (A-2). The pressure gradient in Eq. (A-2) can be expressed by the force balance of the gas core as follows:

$$V_l=\frac{r^2}{4\mu_l}\left(\frac{dP}{dz}+\rho_l g\sin\beta\right)+C_1\ln r+C_2 \tag{A-2}$$

$$\frac{dP}{dz}=-\frac{4\tau_i}{D-2\delta_u}-\rho_g g\sin\beta \tag{A-3}$$

where τ_i is the interfacial shear stress in Pa, δ_u is the uniform film thickness (m), and ρ_g is the gas core density (kg/m^3).

Substituting Eq. (A-3) into Eq. (A-2), we obtain a general expression for the velocity distribution of the liquid film, as shown in Eq. (A-4), where C_1 and C_2 are undetermined coefficients that should be determined by the boundary conditions.

$$V_l=\frac{r^2}{4\mu_l}\left(-\frac{4\tau_i}{D-2\delta_u}+(\rho_l-\rho_g)g\sin\beta\right)+C_1\ln r+C_2 \tag{A-4}$$

The boundary conditions of the nonslip and zero wall shear are presented in Eqs. (A-5) and (A-6), respectively:

$$V_l|_{r=R}=0 \tag{A-5}$$

$$-\mu_l\frac{dV_l}{dr}|_{r=R}=\tau_w=0 \tag{A-6}$$

Substituting the boundary conditions in Eqs. (A-5) and (A-6) into Eq. (A-4), the film velocity distribution is given by Eq. (A-7).

$$V_l=\frac{\left(-\frac{4\tau_i}{D-2\delta_u}+(\rho_L-\rho_G)g\sin\beta\right)}{4\mu_l}\left(r^2-R^2+2R^2\ln\frac{R}{r}\right) \tag{A-7}$$

Integrating the liquid velocity distribution in the range of film thickness, the volume flow rate of the liquid film is expressed as

$$V_{sl}\frac{\pi D^2}{4}=\int_{R-\delta_u}^{R}2\pi r V_l dr \tag{A-8}$$

Substituting Eq. (A-7) into Eq. (A-8), the expression of interfacial shear is presented in Eq. (A-9) in a dimensionless form. Then, other formulations in the simplified model, as well as the expressions of dimensionless parameters, can be found in Section 2.2.

$$\widetilde{V_{sl}}=2\sin\beta\left[1-4\left(\widetilde{\delta_u}-\widetilde{\delta_u}^2\right)\right]\left(\frac{1}{64}-\frac{1}{4}\left(\frac{1}{2}-\widetilde{\delta_u}\right)^4-\frac{1}{4}\left(\frac{1}{2}-\widetilde{\delta_u}\right)^2\ln\frac{1}{1-2\widetilde{\delta_u}}\right) \tag{A-9}$$

Appendix B. - Derivation of the unified model

The nonslip condition at the pipe wall is given by Eq. (B-1). The interfacial shear stress is given by Eq. (B-2), where R is the pipe radius (m).

$$V_L|_{r=R}=0 \tag{B-1}$$

$$-\mu_l\frac{dV_L}{dr}|_{r=R-\delta_u}=\tau_i \tag{B-2}$$

Introducing Eqs. (B-1) and (B-2) into Eq. (A-4), the velocity of the liquid film is expressed as

$$V_l = \frac{\left(-\frac{4\tau_i}{D-2\delta_u} + (\rho_l - \rho_g)g\sin\beta\right)}{4\mu_l}(r^2 - R^2) + \frac{(R-\delta_u)^2}{2\mu_l}(\rho_l - \rho_g)g\sin\beta\ln\frac{R}{r} \tag{B-3}$$

Integrating Eq. (B-3) in the range of film thickness, the volume flow rate of the liquid film is expressed as

$$V_{sl}\frac{\pi D^2}{4} = \int_{R-\delta_u}^{R} 2\pi r V_L dr \tag{B-4}$$

where V_{sl} is the superficial liquid velocity (m/s), and D is the pipe inner diameter (m).

Substituting Eq. (B-3) into Eq. (B-4), the expression of interfacial shear is presented in Eq. (B-5) in a dimensionless form. The definition of dimensionless parameters can be found in Section 2.2.

$$\widetilde{\tau_i} = \frac{(1-2\widetilde{\delta_u})}{2(\widetilde{\delta_u} - \widetilde{\delta_u}^2)^2}\widetilde{V_{sl}} + \sin\beta(1-2\widetilde{\delta_u})\left\{\frac{1}{4} + \frac{(1-2\widetilde{\delta_u})^2\left[(1-2\widetilde{\delta_u})^2\ln\frac{1}{1-2\widetilde{\delta_u}} - 2(\widetilde{\delta_u} - \widetilde{\delta_u}^2)\right]}{16(\widetilde{\delta_u} - \widetilde{\delta_u}^2)^2}\right\} \tag{B-5}$$

By equating the derivative of Eq. (B-5) with respect to $\widetilde{\delta_u}$ to zero, we have the expression of the critical film thickness, as shown in Eq. (B-6).

$$\widetilde{V_{Sl}} = \sin\beta\frac{2(\widetilde{\delta_u} - \widetilde{\delta_u}^2)(2\widetilde{\delta_u}^4 - 4\widetilde{\delta_u}^3 + 7\widetilde{\delta_u}^2 - 5\widetilde{\delta_u} + 1) + \ln\frac{1}{1-2\widetilde{\delta_u}}(\widetilde{\delta_u}^2 - \widetilde{\delta_u} - 1)(2\widetilde{\delta_u} - 1)^4}{8(3\widetilde{\delta_u}^2 - 3\widetilde{\delta_u} + 1)} \tag{B-6}$$

After the uniform thickness (δ_u) is obtained, it should be modified to consider the non-uniform film thickness in inclined pipes. The correction process is as follows.

(a) First, a uniform film thickness (δ_u) is assumed, which can be calculated by Eq. (B-6). The schematic of δ_u is shown in Fig. B-1(a).

(b) In inclined pipes, the film around the pipe wall has a non-uniform distribution, as depicted in Fig. B-1(b). Hence, the uniform thickness (δ_u) should be transferred to the maximum thickness (δ_{max}), in which the liquid film is prone to reverse initially. S. Luo et al. (2014) proposed a simple method to describe the film thickness distribution in inclined pipes by assuming that the area of the non-uniform film is equal to that of an expanded rectangle. Thus, the maximum film thickness can be expressed as Eq. (B-7), which is derived by treating the uniform film thickness as equal to the average maximum and minimum film thickness.

$$\widetilde{\delta}_{max} = \frac{2\widetilde{\delta_u}}{1 + \frac{\delta_{min}}{\delta_{max}}} \tag{B-7}$$

where $\widetilde{\delta}_{max}$ is the dimensionless maximum film thickness; and $\frac{\delta_{min}}{\delta_{max}}$ is the ratio between the minimum and maximum thickness. In this paper, a new empirical relation of $\frac{\delta_{min}}{\delta_{max}}$ is proposed based on a recently published experimental work on film thickness in inclined pipes (Freshtman et al., A. 2020), as shown presented in Eq. (B-8).

$$\frac{\delta_{min}}{\delta_{max}} = \exp\left[-3.44\times10^{-2}(90-\beta)\right] \tag{B-8}$$

Then, the maximum interfacial shear ($\widetilde{\tau}_{max}$) at the maximum film thickness ($\widetilde{\delta}_{max}$) can be calculated using Eq. (B-9), which is derived by combining Eqs. (B-5) and (B-6).

$$\widetilde{\tau}_{max} = \sin\beta\left(1-2\widetilde{\delta}_{max}\right)^3\left[\frac{\ln\frac{1}{1-2\widetilde{\delta}_{max}}\left(1-2\widetilde{\delta}_{max}\right)^2 + 2\left(\widetilde{\delta}_{max}^2 - \widetilde{\delta}_{max}\right)}{4\left(\widetilde{\delta}_{max}^2 - \widetilde{\delta}_{max}\right)\left(3\widetilde{\delta}_{max}^2 - 3\widetilde{\delta}_{max} + 1\right)}\right] \tag{B-9}$$

(c) Finally, by introducing $\widetilde{\tau}_{max}$ back to Eq. (B-5), the equivalent film thickness $\widetilde{\delta_{eq}}$ can be obtained, as shown in Fig. B-1(c). Substituting the maximum interfacial shear at the bottom ($\widetilde{\tau}_{max}$) and the equivalent film thickness ($\widetilde{\delta_{eq}}$) into Eq. (B-10), the critical gas velocity of the film reversal can be calculated. Wallis's (1969) interfacial friction factor is used in Eq. (B-10)

$$\widetilde{V_{sg}} = \sqrt{\frac{2\widetilde{\tau_i}(1-2\widetilde{\delta_u})^4}{f_i}} \tag{B-10}$$

In the unified model, Wallis's (1968) correlation of droplet entrainment fraction is used, as shown in Eq. (B-11). The inception velocity of droplet entrainment is calculated by Eq. (B-12) (Berna et al., 2014). It should be noted that the gas core density and liquid superficial velocity should consider

the droplet entrainment fraction.

$$E = 1 - \exp\left\{ -0.125\left[\frac{10^4 V_{sg}\mu_G}{\sigma}\left(\frac{\rho_G}{\rho_L}\right)^{0.5} - 1.5\right]\right\} \tag{B-11}$$

$$V_d = \sqrt{\frac{9.61\sqrt{\sigma g \rho_l}}{\rho_g}} \tag{B-12}$$

where E is the droplet entrainment fraction, μ_G is the gas viscosity (Pa·s), ρ_G is the gas density (kg/m^3), V_d is the inception velocity of droplet entrainment (m/s), and σ is the surface tension (N/m).

In summary, this solution procedure of the unified model is depicted in Fig. B-2.

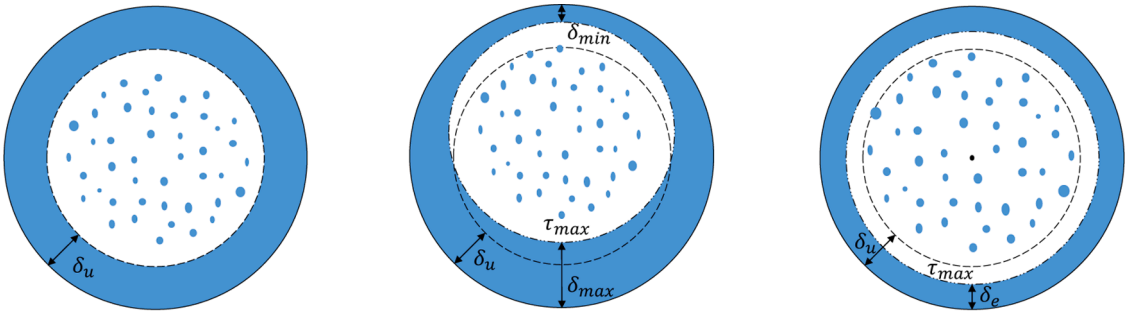

(a) Uniform film thickness (b) Non-uniform film thickness (c) Equivalent film thickness

Fig. B-1. Correction of non-uniform liquid film thickness in inclined pipes.

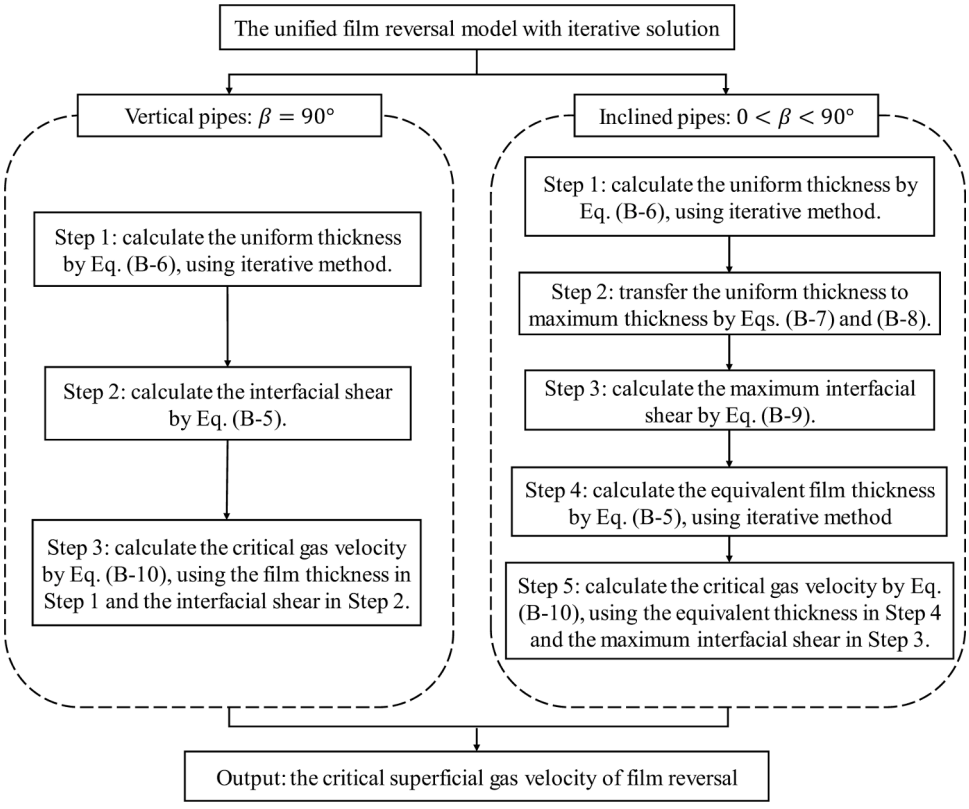

Fig. B-2. The solution procedure of the unified model.

References

Alsaadi, Y., Pereyra, E., Torres, C., Sarica, C., 2015. Liquid loading of highly deviated gas wells from 60° to 88°. In: SPE Annual Technical Conference and Exhibition. Houston, Texas, USA. https://doi.org/10.2118/174852-MS. September.

Andritsos, N., Hanratty, T.J., 1987. Influence of interfacial waves in stratified gas-liquid flows. AIChE J. 33, 444–454. https://doi.org/10.1002/aic.690330310.

Alves, M.V.C., Waltrich, P.J., Gessner, T.R., Falcone, G., Barbosa, J.R., 2017. Modeling transient churn-annular flows in a long vertical tube. Int. J. Multiphase Flow 89, 399–412. https://doi.org/10.1016/j.ijmultiphaseflow.2016.12.001.

Barbosa, J.R., Hewitt, G.F., König, G., Richardson, S.M., 2002. Liquid entrainment, droplet concentration and pressure gradient at the onset of annular flow in a vertical pipe. Int. J. Multiphase Flow 28, 943–961. https://doi.org/10.1016/S0301-9322(02)00003-4.

Barnea, D., 1986. Transition from annular flow and from dispersed bubble flow—Unified models for the whole range of pipe inclinations. Int. J. Multiphase Flow 12, 733–744. https://doi.org/10.1016/0301-9322(86)90048-0.

Belfroid, S.P.C., Schiferli, W., Alberts, G.J.N., Veeken, C.A.M., Biezen, E., 2008. Prediction onset and dynamic behaviour of liquid loading gas wells. In: SPE Annual Technical Conference and Exhibition. https://doi.org/10.2118/115567-MS. September.

Belt, R.J., Van't Westende, J.M.C., Portela, L.M., 2009. Prediction of the interfacial shear-stress in vertical annular flow. Int. J. Multiphase Flow 35, 689–697. https://doi.org/10.1016/j.ijmultiphaseflow.2008.12.003.

Berna, C., Escrivá, A., Muñoz-Cobo, J.L., Herranz, L.E., 2014. Review of droplet entrainment in annular flow: interfacial waves and onset of entrainment. Prog. Nucl. Energy 74, 14–43. https://doi.org/10.1016/j.pnucene.2014.01.018.

Coleman, S.B., Clay, H.B., McCurdy, D.G., Norris, L.H.I., 1991. A new look at predicting gas-well load-up. J. Pet. Technol. 43, 329–333. https://doi.org/10.2118/20280-PA.

Fan, Y., Pereyra, E., Sarica, C., 2018. Onset of liquid film reversal in upward-inclined pipes. SPE J. 23, 1630–1647. https://doi.org/10.2118/191120-PA.

Fershtman, A., Robers, L., Prasser, H.-.M., Barnea, D., Shemer, L., 2020. Interfacial structure of upward gas–liquid annular flow in inclined pipes. Int. J. Multiphase Flow 132, 103437. https://doi.org/10.1016/j.ijmultiphaseflow.2020.103437.

Fore, L.B., Beus, S.G., Bauer, R.C., 2000. Interfacial friction in gas-liquid annular flow: analogies to full and transition roughness. Int. J. Multiphase Flow 26 (11), 1755–1769. https://doi.org/10.1016/S0301-9322(99)00114-7.

Guner, M., Pereyra, E., Sarica, C., Torres, C., 2015. An experimental study of low liquid loading in inclined pipes from 90° to 45°. In: SPE Production and Operations Symposium. Oklahoma City, Oklahoma, USA. https://doi.org/10.2118/173631-MS. March.

Guo, B., Ghalambor, A., Xu, C.C., 2006. A systematic approach to predicting liquid loading in gas wells. SPE Prod. Oper. 21 (01), 81–88. https://doi.org/10.2118/94081-PA.

Lea, J.F., Nickens, H.V., 2004. Solving gas-well liquid-loading problems. J. Pet. Technol. 56 (04), 30–36. https://doi.org/10.2118/72092-JPT.

Li, J., Almudairis, F., Zhang, H., 2014. Prediction of critical gas velocity of liquid unloading for entire well deviation. In: International Petroleum Technology Conference. Kuala Lumpur, Malaysia. https://doi.org/10.2523/IPTC-17846-MS. December.

Liu, Y., Luo, C., Zhang, L., Liu, Z., Xie, C., Wu, P., 2018. Experimental and modeling studies on the prediction of liquid loading onset in gas wells. J. Nat. Gas Sci. Eng. 57, 349–358. https://doi.org/10.1016/j.jngse.2018.07.023.

Luo, S., 2013. Inception of Liquid Loading in Gas Wells and Possible Solutions. Dissertation. The University of Tulsa.

Luo, S., Kelkar, M., Pereyra, E., Sarica, C., 2014. A new comprehensive model for predicting liquid loading in gas wells. SPE Prod. Oper. 29, 337–349. https://doi.org/10.2118/172501-PA.

Magrini, K.L., Sarica, C., Al-Sarkhi, A., 2012. Liquid entrainment in annular gas/liquid flow in inclined pipes. SPE J. 17 (02), 617–630. https://doi.org/10.2118/134765-PA.

Nosseir, M.A., Darwich, T.A., Sayyouh, M.H., Sallaly, M.E.I., 2000. A new approach for accurate prediction of loading in gas wells under different flowing conditions. In: SPE Production Operations Symposium. https://doi.org/10.2118/37408-MS. March.

Pagou, A., Wu, X., Zhu, Z., Peng, L., 2020. Liquid film model for prediction and identification of liquid loading in vertical and inclined gas wells. J. Petrol. Sci. Eng. 188, 106896 https://doi.org/10.1016/j.petrol.2019.106896.

Paz, R.J., Shoham, O., 1999. Film-thickness distribution for annular flow in directional wells: horizontal to vertical. SPE J. 4 (02), 83–91. https://doi.org/10.2118/56233-PA.

Rastogi, A., Fan, Y., 2020. Experimental and modeling study of onset of liquid accumulation. J. Nat. Gas Sci. Eng. 73, 103064 https://doi.org/10.1016/j.jngse.2019.103064.

Shekhar, S., Kelkar, M., Hearn, W.J., Hain, L.L., 2017. Improved prediction of liquid loading in gas wells. SPE Prod. Oper. 32, 539–550. https://doi.org/10.2118/186088-PA.

Skopich, A., Pereyra, E., Sarica, C., Kelkar, M., 2015. Pipe-diameter effect on liquid loading in vertical gas wells. SPE Prod. Oper. 30, 164–176. https://doi.org/10.2118/164477-PA.

Turner, R.G., Hubbard, M.G., Dkuler, A.E., 1969. Analysis and prediction of minimum flow rate for the continuous removal of liquids from gas wells. J. Pet. Technol. 21 (11), 1475–1482. https://doi.org/10.2118/2198-PA.

Tang, H., Sun, Z., He, Y., Chai, Z., Hasan, A.R., Killough, J., 2019. Investigating the pressure characteristics and production performance of liquid-loaded horizontal wells in unconventional gas reservoirs. J. Petrol. Sci. Eng. 176, 456–465. https://doi.org/10.1016/j.petrol.2019.01.072.

Taitel, Y., Barnea, D., Dukler, A.E., 1982. A film model for the prediction of flooding and flow reversal for gas-liquid flow in vertical tubes. Int. J. Multiphase Flow 8, 1–10. https://doi.org/10.1016/0301-9322(82)90002-7.

van 't Westende, J.M.C., Kemp, H.K., Belt, R.J., Portela, L.M., Mudde, R.F., Oliemans, R.V.A., 2007. On the role of droplets in cocurrent annular and churn-annular pipe flow. Int. J. Multiphase Flow 33, 595–615. https://doi.org/10.1016/j.ijmultiphaseflow.2006.12.006.

Veeken, C.A.M., Hu, B., Schiferli, W., 2009. Transient multiphase flow modeling of gas well liquid loading. In: SPE Offshore Europe Oil and Gas Conference and Exhibition. Aberdeen, UK. https://doi.org/10.2118/123657-MS. September.

Wallis, G.B., 1968. Phenomena of liquid transfer in two-phase dispersed annular flow. Int. J. Heat Mass Tran. 11 (4), 783–785. https://doi.org/10.1016/0017-9310(68)90081-1.

Wallis, G.B., 1969. One-Dimensional Two-phase Flow. McGraw-Hill, Columbus, Ohio first ed.

Waltrich, P.J., Posada, C., Martinez, J., Falcone, G., Barbosa, J.R., 2015a. Experimental investigation on the prediction of liquid loading initiation in gas wells using a long vertical tube. J. Petrol. Sci. Eng. 26, 1515–1529. https://doi.org/10.1016/j.jngse.2015.06.023.

Waltrich, P.J., Falcone, G., Barbosa, J.R., 2015b. Liquid transport during gas flow transients applied to liquid loading in long vertical pipes. Exp. Therm. Fluid Sci. 68, 652–662. https://doi.org/10.1016/j.expthermflusci.2015.07.004.

Wang, Z., Guo, L., Zhu, S., Nydal, O.J., 2018. Prediction of the critical gas velocity of liquid unloading in a horizontal gas well. SPE J. 23, 328–345. https://doi.org/10.2118/189439-PA.